TREATMENT OF STANDARDIZED FEMORAL OSTEOTOMIES USING EXTRACORPOREAL SHOCKWAVE THERAPY (ESWT)

by

Feride Şermin Utku – Bilgen

B.A., Biochemistry, ID.
Earlham College, USA, 1985

Submitted to the Institute of Biomedical Engineering
in partial fulfillment of the requirements
for the degree of
Master of Science
in
Biomedical Science

Bogazici University Library
39001101317454

Boğaziçi University
June 18, 2001

ACKNOWLEDGMENTS

I would first like to thank my thesis advisors, Assoc. Prof. Dr. Ahmet Ademoğlu and Dr. Aykut Sümer for their support and encouragement, for helping me through decisions, and always asking the right questions at the right time.

I would like to thank my family members, who have kindly taken over the care of my daughter, Melodi. I would like to thank especially my aunt Oya Coral, who has selflessly worked probably as much as I have done, and my mother, Şükûfe Utku.

I would like to thank Assoc. Prof. Dr. Mehmed Özkan, Dr. Faik Oktar, Prof. Dr. Gönül Sultuybek, Prof. Dr. Tuncay Altuğ, orthopaedic surgeons Nurettin Heybeli, Hayrettin Kesmezacar, and Tahir Öğüt, Dr.s Burak Başarır, Ercan Karaarslan, Hakan Sayrak, and Feza Korkusuz for their extensive contribution to this work, and Prof. Dr. Yorgo İstefanopulos, Assoc. Prof. Dr. Hale Saybaşılı, Dr. Burak R. Arslan, Tolga Taner, and the secreteriat of the Biomedical Engineering Institute for their kind support.

I would like to thank my friends and the assistants at the Institute for sharing with not only the 'psyching' atmosphere of BM 118, but also their friendship and support. Life here would be less meaningful without the concertos of Bach, the numerous aquaria with schools of fish, Guyton as our mentor, our roaming profiles, mugs of tea, and the many coffee, tea and chocolate coco breaks at the Kantin.

TREATMENT OF STANDARDIZED FEMORAL OSTEOTOMIES USING EXTRACORPOREAL SHOCKWAVE THERAPY (ESWT)

ABSTRACT

ESWT is used in treatment of pseudoarthrosis and may also be considered for distraction osteogenesis (callus lengthening) operations. In this study, effects of ESWT on the callus were studied. On 20 male, ten-week-old white Wistar rats transverse femoral osteotomies were performed at mid-diaphysis, and internally fixated with Kirschner wires. At the end of the third week, animals, randomly divided into two groups, underwent ESWT with 1500 (Group I) and 500 (Group II) shockwaves/treatment at a generating voltage of 10 kV on their right femurs; left femurs were used as controls. At the end of the ninth week, animals were sacrificed. Both femurs were examined using X-Ray, computerized tomography (CT), Dual Energy X-Ray Absorptiometry (DEXA), and histological methods. X-Ray data showed that Group I femurs displayed a higher percentage of nonunions and secondary axial displacements than Group II. Group II had a higher percentage of unions and fewer secondary axial displacements than Group I. CT data showed that ESW treated right legs in both groups had a greater callus area, and lower average density of image pixel than controls. In the DEXA analysis of Group II, although there was no significant difference in neither the bone mineral content (BMC) nor the bone mineral density (BMD) between the treated and untreated bones; the treated femurs had a slightly lower mineral content and mineral density than the untreated femurs. The histological score of Group II was considerably higher than that of Group I. In agreement with other studies done on bone healing, the exuberant amount of callus observed after ESWT did not correlate with the level of bone healing.

Keywords - Bone, femur, callus, X-Ray, CT, DEXA, histology, rat.

STANDART FEMUR OSTEOTOMİLERİNİN EKSTRAKORPORAL ŞOK DALGASI TERAPİSİYLE (ESWT) TEDAVİSİ

ÖZET

Ekstrakorporal şok dalgası terapisi (ESWT) psödoartroz tedavilerinde kullanılmakta ve distraksiyon osteogenez (kallus uzatma) ameliyatlarında da kullanılabileceği öngörülmektedir. Bu çalışmada ESWT'nin kallus üzerindeki etkileri incelendi. Yirmi adet on haftalık erkek beyaz Wistar sıçanının diyafiz bölgesinde transverse femoral osteotomi yapılıp, Kirschner teliyle medullar fiksasyon uygulandı. Üçüncü haftanın sonunda sıçanlar iki gruba rastgele ayrılarak, sağ femurlarına 10 kV çıkış voltajında, tek seansta 1500 (Grup I) ve 500 (Grup II) şokdalgası uygulandı; sol bacaklar kontrol olarak kullanıldı. Dokuzuncu haftanın sonunda sıçanlar feda edildi. Her iki femur da radyografi, bilgisayarlı tomografi (BT), kemik densitometri (DEXA) ve histolojik yöntemle incelendi. X-Ray analizlerinde Grup I'deki femurlarda kaynamamış ve ikincil açı oluşturmuş kemik oranının Grup II'den daha yüksek olduğu görüldü. Grup II'de kaynamış kemik yüzdesi Grup I'e göre daha yüksekti ve daha az sayıda ikincil açı oluşturmuş kemik vardı. BT verileri, her iki grupta da, kontrollere kıyasla ESWT uygulanmış sağ femurlarda kallusun alanının daha büyük ve görüntü piksel ortalamasının daha düşük olduğunu gösterdi. DEXA incelemeleri, Grup II'de tedavi edilmiş ve edilmemiş kemikler arasında kemik mineral miktarında (KMM) ve kemik mineral yoğunluğunda (KMY) önemli bir farklılık göstermemekle birlikte, tedavi edilmiş femurların KMM ve KMY değerlerinin kontrol grubundan biraz daha düşük olduğunu gösterdi. Grup II'nin histoloji skorları, Grup I'in skorlarından belirgin miktarda yüksekti. İyileşmekte olan kemik üzerine yapılan diğer çalışmalarla uyumlu olarak, ESWT sonrasında görülen yüksek miktardaki kallusla kemik iyileşme düzeyi arasında önemli bir bağlantı olmadığı görüldü.

Anahtar Kelimeler – Kemik, femur, kallus, röntgen, BT, DEXA, histoloji, sıçan.

TABLE OF CONTENTS

LIST OF FIGURES

LIST OF TABLES

LIST OF ABBREVIATIONS

BMC	bone mineral content
BMD	bone mineral density
BT	bilgisayarlı tomografi
CT	computerized tomography
DEXA	dual energy X-Ray absorptiometry
ESWT	extracorporeal shock wave therapy
EŞDT	ekstrakorporal şok dalgası tedavisi
KMM	kemik mineral miktarı
KMY	kemik mineral yoğunluğu
ROI	region of interest

1. INTRODUCTION

1.1 Historical Background of the Problem

In the recent decades, physical influences have been shown to promote healing in biological systems. Electrical stimulation, electromagnetic fields, piezoelectricity, ultrasound, and mechanical influences have been tested on their effects on bone growth and bone healing. However, the mechanisms of stimulation of bone growth and wound repair are not clearly understood. It has been proposed that cell proliferation, or a faster remodeling of the treated tissue may be related to a second messenger system, to the functional and structural changes of membrane proteins, or release of activators of cell activity by the induced effect of physical forces [1].

Extracorporeal Shock Wave Therapy (ESWT) has demonstrated drastic effects on living tissues, blood vessels, nerves, renal tissue [2-5] and skeletal structures [6]. It is suggested that it acts by creating a cavitation effect on the exposed tissue, and causing hemorrhages [2-5,7,8]. Its suitability for use in treatment of cancer has also been studied [2,7,8]. ESWT treatment of peudoarthrosis has a very high success rate of 60-80% [1,8-18].

Pseudoarthosis (nonunion) is a disorder of the bone healing process, where, instead of the deposition of callus necessary for stabilization and stiffening, the body forms only a cartilaginous link between the fractured bone ends. It is thought that pseudoarthrosis is caused by inadequate blood supply to the bone ends, which enhances formation of chondroblastic progenitor cells [18,19], forming a cartilaginous link at the bone ends which leads to a nonunion.

Before beginning ESWT, patients with pseudoarthrosis need to have tried conservative methods of therapy, i.e. previously unsuccessful treatment or surgery, for at least six months after initial treatment of the fracture. Treatment of pseudoarthrosis by conventional methods is sometimes a very long and expensive process. Some of the patients need to have up to ten

operations before they are successfully treated with ESWT [15]. These long and repeated attempts of conventional therapy are economically unfeasible not only for the patient, but also for the various institutions within the health care system.

ESWT is also known to increase callus volume, which is needed in exuberant amounts in distraction osteogenesis (callus lengthening) operations, where the bone ends are pulled apart from each other at a certain distance over time, and the forming gap is filled in with the newly forming callus, thus increasing the final length of bone. The success of callus lengthening operations are dependent on the amount of callus formed as well as adequate vascularization.

1.2 General Objectives

Our study aimed to analyze the effects of extracorporeal shock waves on the forming callus and to provide more data on callus properties after treatment with ESWT. Normally, one treatment session is enough to promote osteogenesis in pseudoarthrosis. However, sometimes several treatment sessions are needed. Our study has implications for both the effect of ESWT on the forming callus if more than one treatment session is used and in distraction osteogenesis operations, where an exuberant amount of callus is needed.

We wanted to challenge the questions about the effects of total energy transmitted into the therapeutic volume by different numbers of shock waves, and the effect of timing of ESW application by, (a) administering two different amounts of shock waves generated at the same voltage, (b) on the callus at the end of the third week.

1.3 Thesis Outline

In Chapter 2, we will be discussing the physical properties of extracorporeal shockwaves, transmission of shock waves, the effects of extracorporeal shock waves on living

tissues, and the medical applications of shock waves. In Chapter 3, we will discuss the composition, structure and development of bone as well as bone healing. We will overview the current theories relating to mechanotransduction in bone and Frost's theory on strain adaptive remodeling of bone. In Chapter 4, we will discuss the materials and methods used in the experiments, and to obtain the results. Our results will be presented in Chapter 5. The analyses of results and discussion will be given in Chapter 6. The thesis ends with conclusions in Chapter 7.

2. EXTRACORPOREAL SHOCK WAVE THERAPY (ESWT)

2.1 Physical Properties of Extracorporeal Shock Waves

A shockwave is a non-linear wave. It has a high-pressure amplitude with a rise time of a few nanoseconds and a frequency spectrum ranging from the audible to the far ultrasonic region. There are three mechanisms for producing shock waves (a) electrohydraulic, (b) electromagnetic, and (c) piezoelectric [20,21] as shown in Figure 2.1.

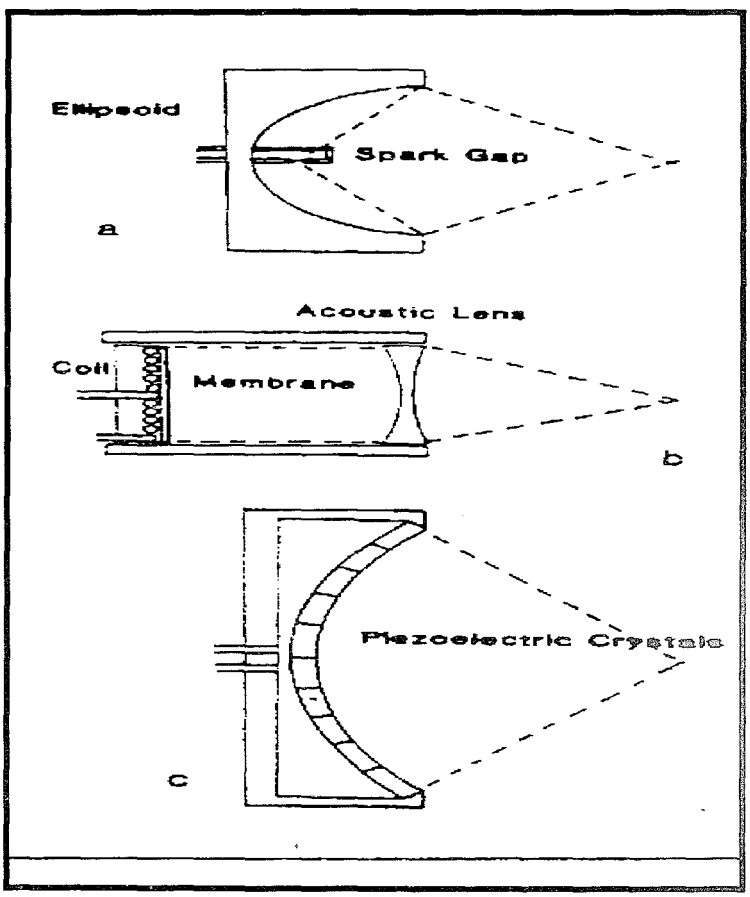

Figure 2.1 Different types of shock wave generators [21].

The electrohydraulic shock wave generator (see Figure 2.2) uses the tip of an electrode, sitting in the focal point of a semiellipsoid, as the point source. High voltage at the tips of the electrode produces a spark, which vaporizes the water and produces spherical shockwaves, which, reflected from the metal ellipsoid are then focused into the patient's body at the second focal area, which is adjusted to therapeutic volume. The focal area of the shockwaves is defined as the area in which 80% of the maximum energy is reached. At 20 kV, the focal area has a length of 60 mm. in the direction of the shock wave axis and a radius of 6 mm in the direction perpendicular to the shock wave axis. The pressure range may vary between 35-49 MPa. Shock wave generation frequency is 30-120/min. Focal energy goes up to 50 mJ [12].

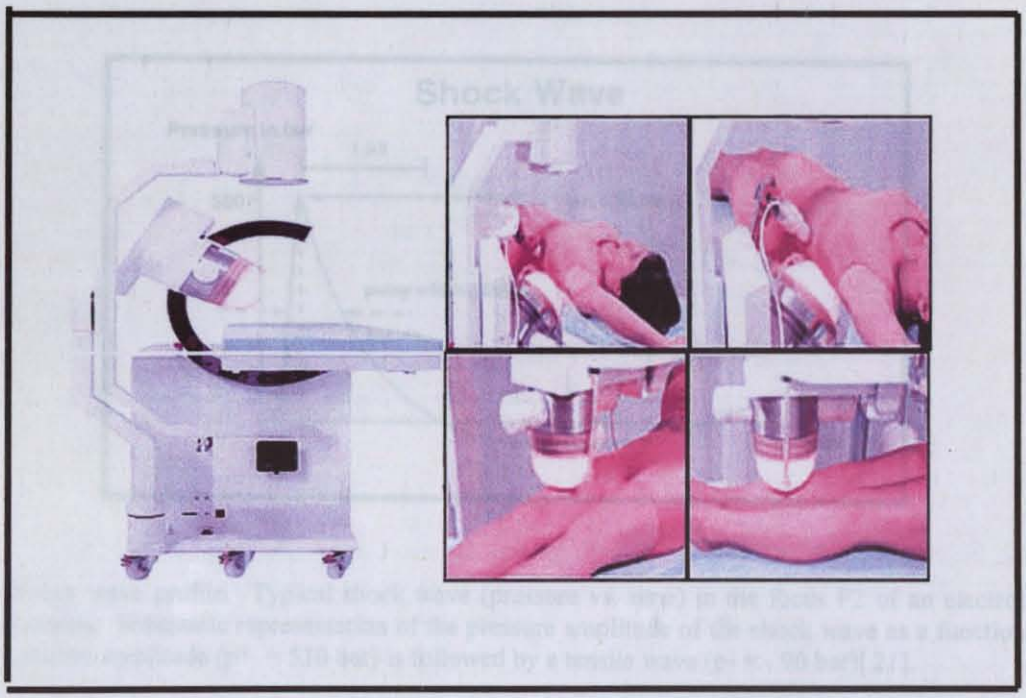

Figure 2.2 PCK Stonelith Litho3pter extracorporeal shock wave device[22].

The electromagnetic shock wave generator uses an electromagnetic coil and a metal membrane. A high current pulse is released through the coil generating a strong magnetic field, inducing a high current in the membrane. The electromagnetic forces accelerate the metal

metal membrane away from the coil, creating a slow and low-pressure acoustical pulse. The waves are focused via an acoustic lens. The focal point is defined by the focal length of the lens. The amplitude of the focused acoustical wave increases non-linearly when the acoustical wave propagates toward the focal point. The rise times of electromagnetically generated shock waves are in the range of a few hundred nanoseconds.

The piezoelectric shock wave generator uses from a few hundred to some thousand piezoelectric crystals mounted on a spherical surface. When switching a high voltage pulse to the crystals, they immediately contract and expand, generating a low-pressure pulse in the surrounding water. The geometrical shape of the sphere focuses the waves. The nonlinear shock wave propagates in increasing amplitudes to the focal point.

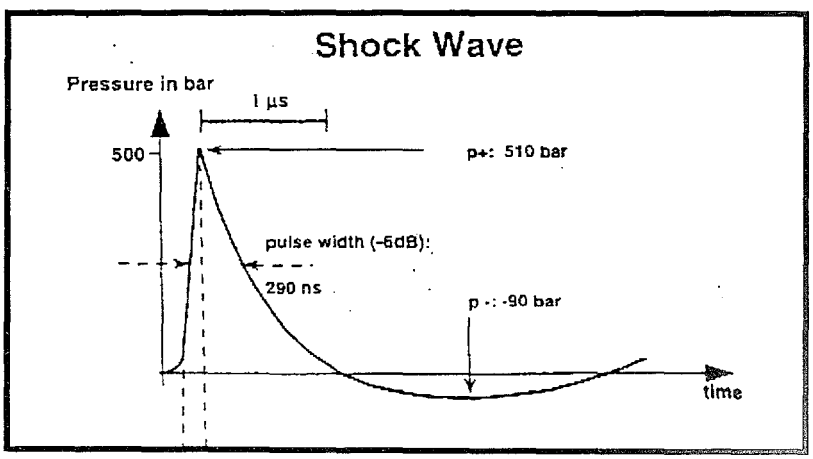

Figure 2.3 Shock wave profile. Typical shock wave (pressure vs. time) in the focus F2 of an electrohydraulic shock wave system. Schematic representation of the pressure amplitude of the shock wave as a function of time. A positive pressure amplitude (p+ = 510 bar) is followed by a tensile wave (p- = - 90 bar)[21].

Shockwave pressure profile (see Figure 2.3) is a single impulse with a wide frequency range from 1 Hz to 20 MHz, high pressure amplitude (up to 120 MPa) and a low tensile amplitude (up to 10 MPa). Rise time of the positive pressure amplitude is non-linear, generally varying between 1-10 ns. The negative pressure following the positive pressure is a

diffraction induced tensile wave of a few μs duration. The pressure profile displays an energy density of up to 1.5 mJ/mm^2 and a pulse energy of up to 100 mJ as determined from its temporal and spatial distribution. The energy density describes the maximum amount of acoustical energy transmitted through an area of 1 mm^2 per pulse. The total pulse energy is the sum of all energy densities across the beam profile multiplied by the area of the beam profile, giving the total acoustic energy per released shockwave. Energies generated in the focal area in vitro are calculated from pressure waveforms by measuring the wave pressure as a function of time at N different radii from the z axis (see Figure 2.4) [4,22]. Peak energy densities of lithotriptors are in the range of 0.1-1 mJ/mm^2, with pulse energies in the range of 10-100 mJ [4].

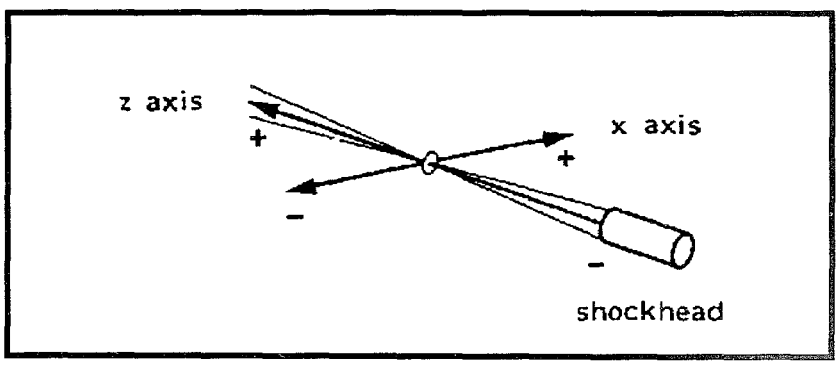

Figure 2.4 Shock wave transmission path. Relation of x and z axes to the focus and the position of the shock wave generator. The z axis resembles the shock wave transmission path (axial direction). The x axis (lateral direction) is perpendicular to the z axis in the focal plane[23].

The total energy per pulse is calculated according to the following equation,

$$E = \frac{1}{\rho c} \sum_{n=1}^{N} \left[\int_0^{\infty} p^2(\tau_n, t) dt \right] A_n \qquad (2.1)$$

where ρ is the density of the medium (water, kg/m^3), c is speed of sound in water (m/s), p is pressure (Pa), r is radius (mm), t is time (seconds), and A_n is the total area in mm^2 [23].

When assessing different shock wave devices, it is not sufficient to compare single parameters, e.g. the maximum energy density. The pressure distribution, the energy density and the total energy in the second focus F2 are the important parameters used to compare different shock wave devices. Each lithotriptor has a specific disintegration capability per shock wave pulse for a certain energy setting. The specific disintegration capability is proportional to the total energy in the shock wave pulse. The disintegrated volume is proportional to the number of applied shock wave pulses. Therefore the disintegrated volume of a lithotriptor could be estimated by the equation $V = \varepsilon E n$, where V is the total disintegrated volume, ε is the specific disintegration capability for a certain material and n is the total number of applied shock waves [21]. Vergunst [23] suggests use of energy within predescribed areas around the focal point, instead of assessment of isobar zones when comparing different lithotriptors.

2.2 Transmission of Shock Waves

When propagating through a tissue, shockwaves face the acoustic resistance of the material they are traveling through. Water, having the same acoustic resistance as that of the shockwaves, provides minimal amount of resistance, absorption and reflection. In soft tissue, its energy is absorbed by 10-20% at a depth of 10 cm. Using a broadband piezoelectric pressure probe connected to an oscilloscope, in vivo pressures can be obtained and recorded. In vivo pressures may be 15% - 25% lower than those measured in vitro [23].

When traveling through a tissue or material that provides high resistance, i.e. kidney stones or bone, some of the shockwave energy is reflected back from the surface of the material and some is reflected back after being absorbed by the material, causing the brittle material to disintegrate into crumbles from its periphery to the center. The shock wave causes high stress forces on the surface of the stone material by the high-pressure amplitude and the

very short time exceeding the elastic strength of the stone material and disintegrating the surface of the stone. Vergunst [23] has measured significantly lower pressures behind focused stones indicating that most of the shock wave energy was absorbed by the stone. Coleman et al. [20], have found that attenuation of shock waves is less dependent on the thickness of tissue layers than assumed, probably due to the absence of important acoustic interfaces between the various types of tissues.

As a shock wave propagates through mediums of different acoustic resistances, at the interface of two mediums, part of the wave is transmitted and part of it is reflected. The ratio of the transmitted intensity, I_T and the reflected intensity, I_R are correlated to the incident intensity by the equation [21]:

$$I_R = I_1[(Z_2 - Z_1)/(Z_2 + Z_1)]^2 \tag{2.2}$$

and

$$I_T = 4I_1Z_1Z_2/(Z_2 + Z_1)^2 \tag{2.3}$$

and

$$I = 2Z/\int p^2 dt \tag{2.4}$$

where I_T is the intensity in medium 2, I_1 in medium 1, $Z = \rho c$ is the acoustical impedance (ρ is the density of the medium and c is the velocity of sound in this medium), Z_1 is the acoustical impedance in medium 1, and Z_2 in medium 2. p describes the pressure amplitude and I corresponds to the acoustical energy density measured in mJ/mm^2.

Table 2.1.
Acoustical data of different tissues[21].

Material	Density (g/cm^3)	Sound Velocity (m/s)	Acoustic Impedance ($g/cm^2s)10^{-5}$
Water	1	1492	1.49
Muscle	1.06	1630	1.72
Fat	0.9	1476	1.37
Cortical Bone	1.8	4100	7.38
Cancellous Bone	1	1450	1.45

When shock waves are focused on the cortical bone, according to Table 2.1, 65% of the incident energy is transmitted to cortical bone, and 35% is reflected. The interface of medium two, the cortical bone under the periosteum, is the site of a strong direct effect of the interaction of the shock waves. This is thought to be the cause of the subperiostal hematoma observed after treatment. According to pressure measurements performed by Graff (1990) in animal bones, there is an 80-90% reduction of energy within only 1 to 2 cm. of cortical bone [21].

2.3 Medical Applications of Extracorporeal Shock Waves

In medicine, shockwaves were first used in urology (lithotripsy). Further applications of ESWT emerged as its possible side effects on blood vessels, nerves and renal tissue were studied. Pelvic bones of tested animals were also exposed to shock waves. Microscopic examination of bones displayed small ruptures and bleeding in bone trabeculae, similar to a fresh fracture. After ESW treatment, a fast rate of bone formation was observed which paralleled an increase in number of osteoblasts [1]. ESWT was also found to promote wound healing at low energies [8,10]. Brümmer et al. [2] and Steinbach et al. [7] studied the effects of ESWT on cancer and found that at increasing energies, cell membrane permeability increases and with the addition of cytostatics, there is a reduction in the number of tumor cells.

The orthopedic applications of shockwaves can be listed as neogenesis of bone tissue and fibrous tissue. At low energies it is used for treatment of calcification in muscles, soft

tissue and tendons and at higher energies for the treatment of fractures and nonunions as listed in Table 2.2 [17]. In the early 1990's, the analgesic effect of shockwaves was discovered and applied first on the shoulder pain. Tendinosis calcarea and tennis elbow, humeroscapularis, and heel spurs, where chronic inflammation due to the calcareous deposits in soft tissues is the cause for the pain, were successfully treated with ESWT [8,23,24]. Patients with tendinopathies were treated with shock waves if they have had three months of prior unsuccessful conservative treatment and were considered for surgery.

Table 2.2.
Treatment conditions for hard and soft tissues[22].

	Hard Tissues	Soft Tissues
Length of Treatment	30-60 min	10-40 min
Number of Shockwaves	2000-4000	500-2000
Repeats	1-2 treatments	1-3 treatments
Pressure	35-51 MPa	35-51 MPa

2.3.1 Treatment of Pseudoarthrosis by ESWT

In orthopaedics, ESWT was first applied to pseudoarthrosis (nonunion), which is a disorder of the bone healing process, where, instead of the deposition of callus necessary for stabilization and stiffening, the body forms only a cartilaginous link between the fractured bone ends. The different types of pseudoarthrosis are shown in Figure 2.5. Treatment of nonunions by ESWT has a high success rate of 60-80% [15,18].

Although the mechanisms of healing by ESWT are not clear, the microscopic examination of bones immediately after treatment displays a selective destruction of osteocytes, microfractures of trabeculae, minor bleeding in the medullary space, small ruptures and bleeding in trabeculae, similar to a fresh fracture; and three weeks after treatment, an increase in number of trabeculae and their cross-linking and a fast rate of bone formation, paralleling an increase in the number of osteoblasts are observed [1,14]. It is thought that at low energy densities, fracture and wound-healing rates may be stimulated; whereas at high energy densities healing rates may be depressed [10,11,15,16].

The mechanism of healing by ESWT is thought to be similar to that of surgery, where the cartilaginous link between the bones is re-injured mechanically by means of a scalpel or other instruments, providing an effect similar to that of a fresh fracture. It is thought that pseudoarthrosis is caused by inadequate blood supply to the bone ends, which enhances formation of chondroblastic progenitor cells [18,19] instead of the osteoblastic cells. The question on the mechanisms of ESWT, may be approached from two levels: physiological and biomechanical. At the physiological level, knowing that bone healing is initiated immediately by inflammation and local subperiosteal bleeding, the inflammation reaction caused by ESWT could thus be the main stimulus to start the sequence of events that lead to osteogenesis. In addition, the fact that ESWT induced osteogenesis without local bleeding has been demonstrated at low energies leads us to search for a biomechanical explanation of the mechanism of ESWT: the dissociating and dispersing effect of ESWT, caused by the immense mechanical energy applied not only on the mineral, but also on the organic component of bone may change the prevalent strain levels in the bone tissue and lead to osteogenesis as explained by the Mechanostat theory of Frost and Jee (see also Figure3.6, section 3.5).

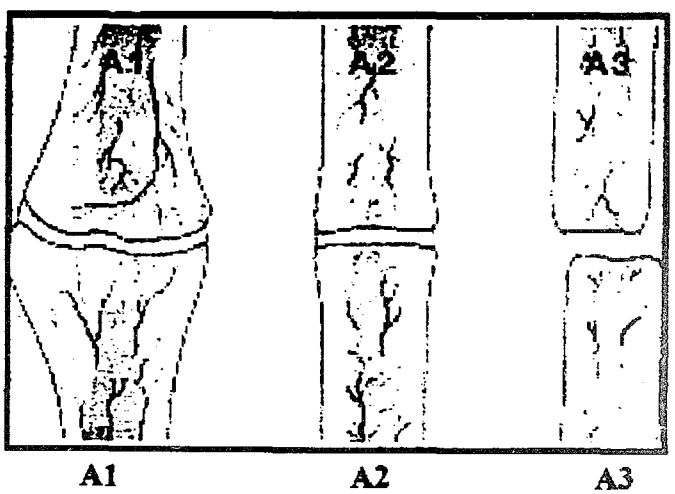

Figure 2.5 Types of pseudoarthrosis. A1: hypertrophic, A2: elephant feet, A3: atrophic[22].

Before beginning ESWT, patients with pseudoarthrosis need to have tried conservative methods of therapy for at least six months. Therapy may be started - in the absence of any metal - if lesion is situated within the diaphyses, if the skin is intact, and if there are no signs

of infection. Treatment success is confirmed generally with callus formation by six weeks. Healing seems to occur more often in hypertrophic nonunions than in atrophic nonunions [9,11].The time required for healing of the nonunion seems to be around that of conventional fracture and dependent on the primary rigidity of the pseudoarthrosis (see section 3.4.2) [15,16].

2.4 Side Effects of Shock Waves

Shockwaves have various biological side effects on tissue and cells. The most important parameters determining the biological effects of ESW are the peak positive pressure and the focal pressure distribution of the lithotriptor. The side effects of shock waves are observed as a function of the total amount of energy absorbed in a certain volume and are proportional to the total mechanical energy delivered by the wave (see Figure 2.6). Brümmer et al. [3] state that hematomas depended on the energy applied rather than the number of shock waves. Haupt et al. [8] state that a certain threshold in energy density (see Figure 2.7) has to be exceeded in order to stimulate the healing processes as well as the side effects and that the sum of biological effect is correlated with the total amount of acoustical energy above a certain threshold.

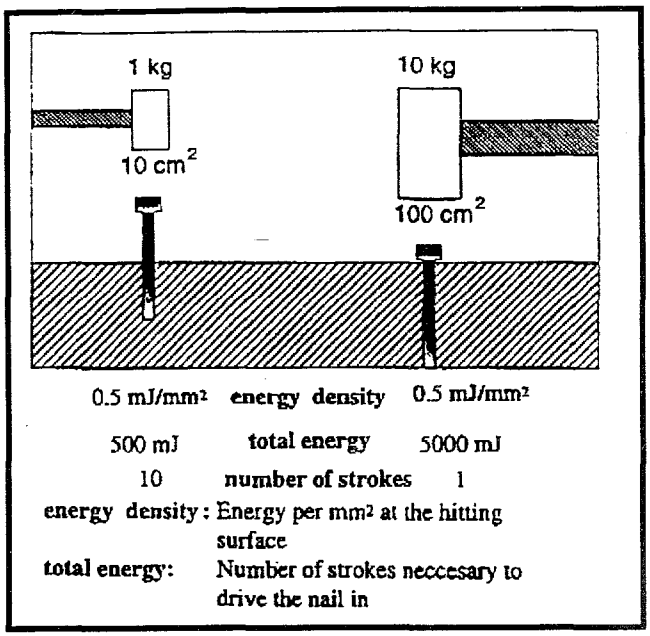

Figure 2.6 Differences between low and high energy generators. Illustration about the difference in effects of a low energy and high energy shock wave device (a small and a big hammer in the figure). Both hammers have identical energy density on the hitting surface of the hammer but a different total mechanical energy which results in different number of strokes to drive the nail in[21].

Cytotoxicity is observed with the increasing number of ESW [7,26]. An increase in cell membrane permeability [7], and damage to cell organelles [2,4] have been described. In 1987, Russo described swollen endoplasmic reticulum, mitochondria with distorted cristae, and separation of nuclear envelope [2]. ESWT has a dispersing, dissociating effect on multicell spheroids in suspension [7]. Cytotoxic effects of ESWT are not observed below a certain threshold level. Steinbach et al. [7] have described the following morphological alterations in the cell: threshold for morphological alterations of the cell skeleton is at 0.21 mJ/mm^2, of the mitochondria is at 0.32 mJ/mm^2. No alterations in tubulin were observed even after 0.32 mJ/mm^2, however, a decrease in nuclear size and significant morphological changes in the nuclear membrane occurred at 0.50 mJ/mm^2.

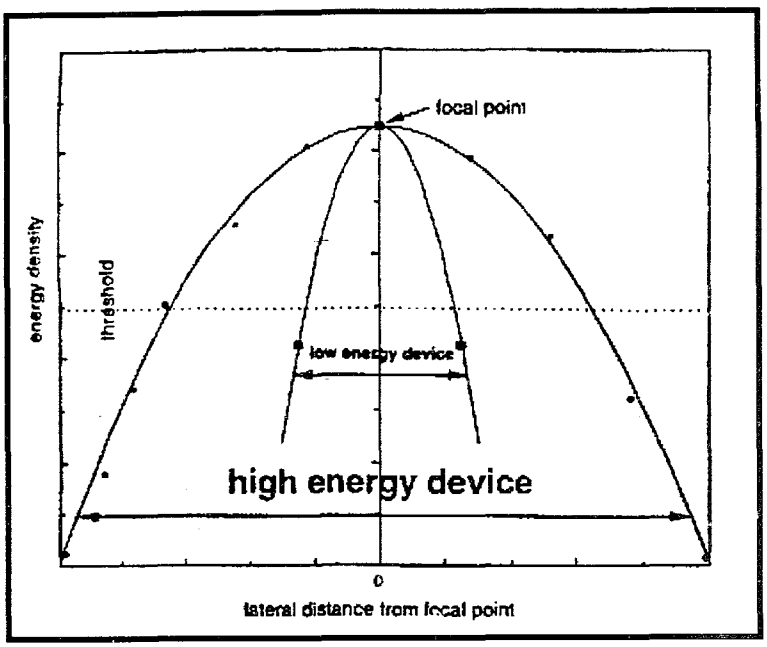

Figure 2.7 Focal pressure distribution for shock wave generator. The focal pressure distribution for a low energy and high energy shock wave device are different. Each generate the same maximum energy density in the focal point but with different pressure distributions (lateral size of focus volume). Therefore, the total amount of pulse energy is different for each case[21].

The negative pressure portion of the shockwave profile produces a cavitation effect, which leads to formation of bubbles in liquid. These bubbles may collapse when they are struck by the positive pressure component of the following shock wave, which is thought to be the probable mechanism of acute tissue injury [21]. Delius [4] and Coleman [20] have described cavitation effect of ESW experimentally at different oxygen concentrations of lithotriptor water bath. In cell suspensions, along with cavitations, jet streams take place due to a local accelaration of the fluid in the focus of shock waves .

Biologically degenerative effects of ESWT may be indirectly mediated by ischemia, but other cytotoxic events at a subcellular and macro molecular level are most likely to occur as well. Shockwaves are not to be used in the presence of hemorrhages, cancer and in the alveolar area of the lung [16]. When used in lithotripsy, side effects can be listed as severe pain, palpalation, hemorrhages, hematurea, damages in kidney paranchymea, ventricular

arythmia, hypertension, and ulsers of stomach, duedonum and colon [4,20]. As a shock wave travels through bone tissue it causes hemorrhages, palpalations, disintegration of bone tissue, and severe pain [2,4]. Immediately after ESWT of skeletal tissue, degeneration of myofibers [27], destruction of osteocytes, microfractures of trabeculae, minor bleeding in the medullary space are observed; about three weeks after exposure, an increase in osteoblasts and thickening of corticalis are seen [14].

2.5 Previous Experiments Performed on Cortical Bone Using ESWT

First research on bones was performed in mid 1980's by Yeaman et al. The first paper concerning the treatment of pseudoarthrosis was written by Valchanov in 1991. Senge, Schleberger, Haupt and Ekkernkamp from Bochum studied ESWT of pseudoarthrosis. Their research showed that in the case of a disturbed bone growth, the positive stimulating effects of shockwave therapy were proven to be effective. In vivo experiments performed at the University of Heidelberg confirmed the findings of the University of Rotterdam that shock wave therapy causes an increased cell division activity. In designing our experiments we used the information provided by the following researchers: Kaulesar et al. [6], Haupt et al. [10], Uslu et al. [28], and McCormack et al. [29]. Let us briefly summarize what research has been done in this field.

Graff, et al. (1989) treated the left spina iliacha anterior superior and left femur distal of rabbits at 1500 sw/treatment at 20 kV and 25 kV. Animals were sacrificed at 48 hrs., two and three weeks after ESWT. Intra and intermuscular hematoma, microscopic periosteal petechial bleeding, but no macroscopic changes were observed in 48 hr. group, where as aseptic necrosis of bone marrow, osteoid damage, excessive osteoneogenesis and callus formation were observed in the two and three week group [10].

Valchanau et al. [18] treated 82 bones in 79 patients with delayed union or nonunion of fractures using a single treatment of ESW at 1000 to 4000 shockwaves with a bone focus of 1000 to 1700 bars. Fractures were immobilized for an average of 81 days. They obtained

85.4% (70 cases) bony union. They state that ESWT breaks up the sclerotic bone ends, producing microfissures, and enhancing blood supply. The production of numerous small, detached fragments of bone exerts a stimulating effect on osteogenesis which leads to a union.

Ekkernkamp et al. (1992) treated 42 sheep tibia with standardized osteotomies with ESW using 3000 sw/treatment at 20-24 kV on the seventh day after the operation. After a seven week healing period, treated bones displayed higher mechanical strength and lamellar bone formation [1].

Haupt et al. [16] studied the effect of ESW on fracture healing in rats. Animals underwent five treatments of ESW on days 2, 5, 9, 14, and 19 after fracture at 100 sw/treatment at 14 or 18 kV. Bone weight, breaking strength, radiology, Calcium-45 uptake and histology were used as analytical parameters. They found significant differences in radiological findings, while histologically no striking differences could be found. The breaking strength of the humeri in the treated group was higher than in the control group. Haupt et al. state that shock waves have a positive effect on fracture healing, and that the treated bones having a lower Calcium-45 uptake are already at a normalized mineralization level, while the untreated group is at a higher remineralization activity.

Haupt et al. [10] used ESW in treatment of wounds, applying 10 to 1000 sw/treatment at 14 and 18 kV. They found a dose dependent influence of shockwaves on wound healing; where high energies inhibited and low energies stimulated re-epithelization. Intermediate energies did not affect the healthy animals, whereas in delayed wound healing intermediate energies accelerated the healing process. Although the mechanisms are unknown, the role of hyperthermia is suspected.

Schleberger et al. [15] treated 37 patients with long-bone nonunions. They used 1200 and 1500 sw/treatment, at 16 kV in cancellous bone, and 18 kV in diaphyses. Giving only a single treatment of ESWT, out of the 33 nonunions that healed, 18 healed with osteosynthesis and 15 without osteosynthesis.

Kaulesar-Sukul et al. [6] studied the relationship between the energy density of the shock waves, the number of shock waves applied and the resulting in vitro effects on cortical bone. At 0.23, 0.33, 0.42, and 0.54 mJ/mm^2 energy densities, they treated 36 rabbit femurs and tibiae. They determined that there is a linear relationship between the energy level of the shockwaves and the severity of the cortical bone defects. They observed the first effects of ESW after 1000-2000 shock waves as bone chipping and gross cortical changes. Effects of ESW gradually severed as the number of shock waves increased, leading to total bone fractures. After 5000 shock waves, there were no further changes [6].

Gündeş [30] treated right femurs of male rabbits at the distal one third proximal to the subchondylar region with ESW at 1000 and 1500 sw/treatment at 18kV. Left femurs were used as controls. He found local bleeding in trabecular bone, bleeding and congestion in the marrow, and focal endosteal bleeding and concluded that ESW has traumatic effects on bone tissue at both 1000 and 1500 sw/treatment at 18kV. In histological studies, he identified basophilic degeneration after the fourth week and a stimulation of the regeneration of the cambium layer.

Johannes et al. [11] using 4000 shock waves of 0.54 mJ/mm^2 (14.5 kV) treated nonunions in two randomized groups of five dogs each. Shock waves were applied on the four preselected sites, on the dorsal and ventral sides of the nonunions. Dogs attained radiographically observable bony union within twelve weeks after ESW treatment, whereas the control group had four radiographically detected nonunions. Johannes et al. conclude that ESWT successfully treats hypertrophic nonunions.

McCormack et al. [29] treated New Zealand rabbit radii using ESW and compared their results with the naturally healing rabbit radii. They state that although ESWT has a local osteogenesis effect, the amount of callus formation does not correlate with accelerated fracture healing, on the contrary, it may retard the remodeling process.

Kuderna et al. [12] and Schaden et al. [14] treated 40 patients with nonunions and fractures with delayed healing. Bony consolidation was achieved in 55% of the patients with a simultaneous decrease in symptoms. Local reactions, such as swelling, hematomas, petechial

hemorrhages were observed. They varied the shock wave intensity and the number of shock waves according to the area of the fracture gap and the cross-section of the bone to be treated. Lower leg and femur were treated with the highest intensity (28 kV) at the maximum number of shock waves (4000).

Russo et al. [13] had 67.2% total fusions, 20.8% partial fusions and 12% no fusions, out of 125 nonunions treated with ESW. In the healing bones they observed vascularization and osteogenesis. They theorized that the hydroxyapatite crystals broken down to smaller pieces, free the microcrystals which behave like calcic aggregation nuclei, thus induce the release of bone morphogenic protein, an osteogenetic factor normally present in bone, but not active because it is covered by the hydroxyapatite macrocrystal. They also stated that mature bone formation may be promoted through osteogenesis, angiogenesis and fibrillogenesis.

Vogel et al. [5] used ESWT in the treatment of 52 patients with pseudoarthrosis and a history of previous conventional therapy. Healing of the pseudoarthrosis was achieved in 61% of the patients at a mean duration of three months. ESWT failed in the treatment of atropic pseudoarthrosis, fibrous dysplasia or osteogenesis imperfecta.

Uslu et al. [28] studied the effect of ESWT on rabbit radii. They created a defect of 1 cm and treated the defect on days 7, 14 and 21 at 1000 sw/treatment at 14 kV. Using CT, DEXA and histology, they concluded that ESWT has a disorganizing and dispersing effect on callus than a direct osteoinductive effect, and suggested that it can be used in bone defects and callus lengthening.

Beutler et al. [9] treated 27 pseudoarthrosis cases, using two treatments of ESWT at 2000 shock waves at 18 kV. Eleven of the cases had undergone osteosynthesis prior to ESWT. Success rate was 41% and radiological evidence of treatment success appeared within six months of therapy. Their data suggests that success of ESWT is inversely proportional to the length of time after conventional pseudoarthrosis treatment.

3. BONE TISSUE AND FRACTURE HEALING

3.1 Composition and Structure of Bone

The skeletal system supports the body (maintaining posture), protects the internal organs (brain and spinal cord), coordinates motility by means of muscles, acts as a systemic mineral source (phosphorus, calcium and others), and produces red and white blood cells. Bone tissue is a dynamic structure that is resorbed, re-formed and remodeled.

Bone is the main building stone of the skeleton. Bone is composed of bone tissue, connective tissues, nerves and blood vessels. The bone matrix consists of collagen fibers, osteocytes, cement substance (mainly mucopolysaccharide) and mineral (mainly hydroxyapatite, an inorganic composition of a yet unknown formulation, consisting mainly of calcium phosphate, calcium carbonate and sodium salts and have a special orientation to the collagen fibers)[31]. Mineral fraction of osseous tissue consists of mainly of calcium, magnesium, potassium, chloride and fluoride. Trace amounts of strontium, lead and other heavy metals may also be found. Some of the inorganic constituent is present as ions in the cement substance, but most of it is present as crystals intimately associated with collagen fibers, or as amorphous calcium phosphate.

Normal adult cortical bone (free of adherent soft parts and thoroughly defatted) is about 5-10% water, 25-30% organic matter, and 65-70% inorganic matter, by weight. Collagen makes up 20-25% of total body protein, and 40% of it is in the bones, in the form of collagen fiber bundles. Collagen makes up 90-95% by weight, of the dry, fat-free organic matter of bone [32]. Bone tissue comprises of cartilage, with collagens and proteoglycans. Recently, cartilage proteins which are thought to have roles ranging from involvement in matrix organization or matrix-cell signalling through to modulation of the chondrocyte phenotype have been described.

3.2 Structure of Compact Bone

On the basis of the arrangements and character of the fiber bundles and the osteocytes, there are two types of bone: compact and cancellous. Cancellous bone is the highly porous, and shock absorbant bone forming the endosteal section of most bones, as well as parts of body on which high loads are placed. Compact bone tissue forms the structural shell of most bones and nearly all of the diaphyses of long bones. In compact bone, collagen fibers are grouped into stratified layers; bone cells are smaller and less numerous and show an orderly arrangement. The collagen fibers in compact bone are arranged concentrically into lamellar sheets (3-7 um. thick), which run helically with respect to the long axis of cylindrical osteons or the Haversian systems (see Figure 3.1), which are arranged within the interstitial or ground lamellae and contain the remains of Haversian systems that have been partially resorbed. They are penetrated by Volkmann's canals, through which nutrient vessels enter the bone to reach the vessels in the Haversian canals. Large numbers of canaliculi pass radially from the canal to the lacunae and intercommunicate with each other. Their function is thought to be the diffusion of nutrient fluids toward the osteocytes and waste products toward the nutrient vessels.

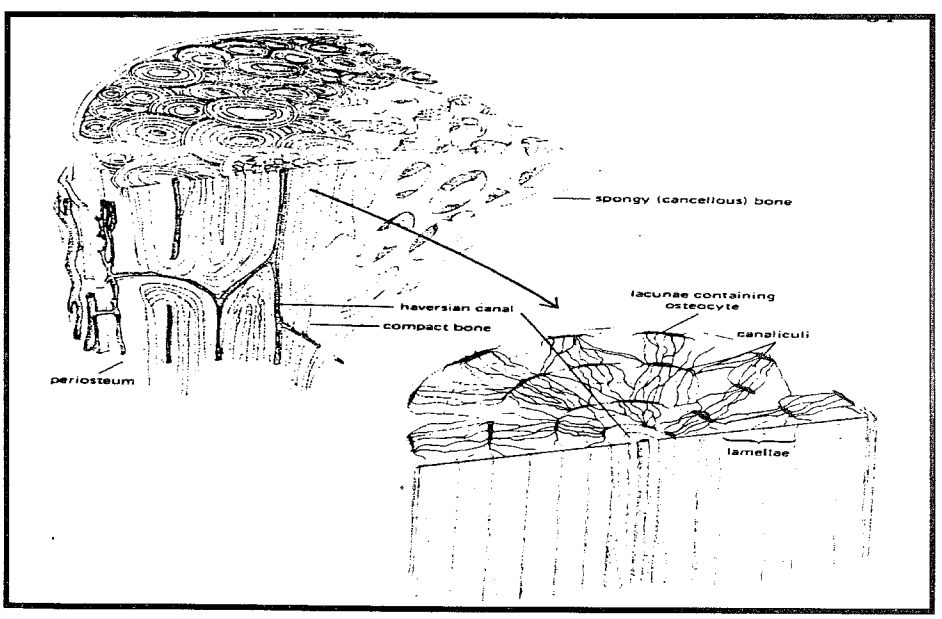

Figure 3.1 The Haversian system[31].

3.2.1 The Rat Femur

The femur (Figure 3.2) is the long and tubular bone of the upper leg. There are two main differences between the human and rat femur: (a) rat epiphyses remain open during the life-time of the animal and longitudinal long bone growth continues, and (b) Haversian remodeling does not normally occur in rats. As in humans, rat bones vary by sex, age and strain and individual [33]. In young rats, the total femoral width and femoral length are associated by the relation TW=1.70+0.07 FL, where TW stands for femoral width, and FL for femoral length. For a given increase in femoral length, young rats have a smaller increment in width than do adult rats. The width of the cortical walls at mid shaft is also highly correlated with femoral length [33].

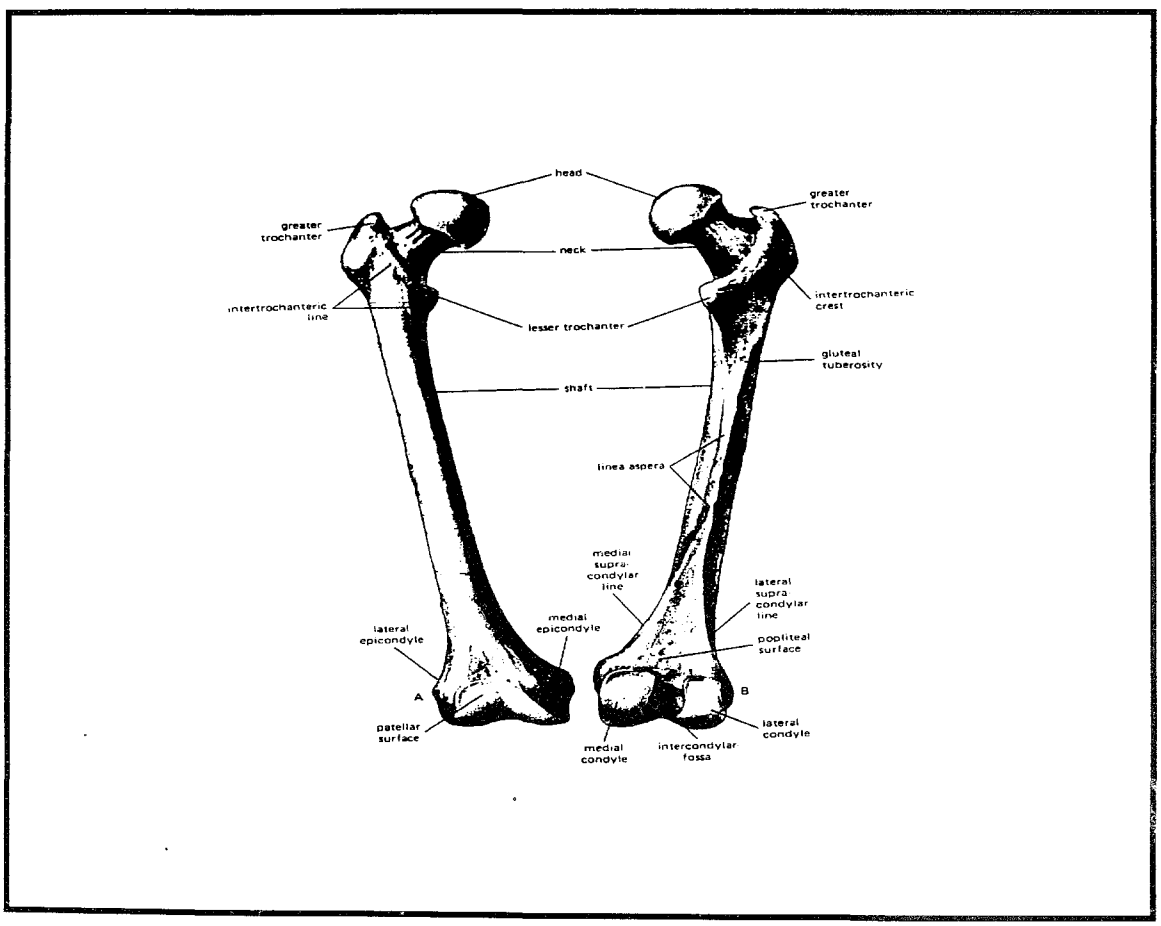

Figure 3.2 The human femur; anterior view, left; posterior view, right[33].

The physical properties of rat bone differ from those of humans and other species. Rat bone has a higher specific gravity and mineral ash content than human bone. Table 3.1 lists the results of hydrated bone assays for different species using cortical bone from the tibia and the femur. The number of adults of each species sampled is indicated in parentheses after the common species name.

Table 3.1.
Physical properties of bone specimen according to species[32].

Species	Specific Gravity	Water Content, vol %	Mineral Ash, vol %	Organic 4 CO2, vol %
Fish (2)	1.80	39.6	29.5	36.9
Polar Bear (1)	1.92	33.0	36.2	40.1
Human (15)	**1.94**	**15.5**	**39.9**	**41.8**
Elephant (1)	2.00	20.0	41.4	41.5
Monkey (3)	2.09	23.0	42.6	41.1
Horse (3)	2.02	25.0	41.0	40.5
Dog (10)	1.94	28.0	38.7	35.5
Cow (5)	2.05	26.2	42.6	36.2
Rabbit (2)	2.12	24.5	45.0	37.2
Rat (12)	**2.24**	**20.2**	**49.9**	**38.3**

3.3 Development of Bone Tissue

Adult bone is a continously remodeled, living organ, where there is a balanced deposition of newly mineralized bone and resorption of old bone. During childhood and adolescence, however, bone is modeled in order to promote growth and to re-shape the bones to adult size and configuration. As a lifelong process, remodeling is controlled by systemic hormones and cytokines, and is an integral part of the calcium homeostatic system. The maintenance of a normal, healthy skeletal mass depends on interactions between osteoblasts, osteoclasts and constituents of the bone matrix to keep the processes of bone resorption and

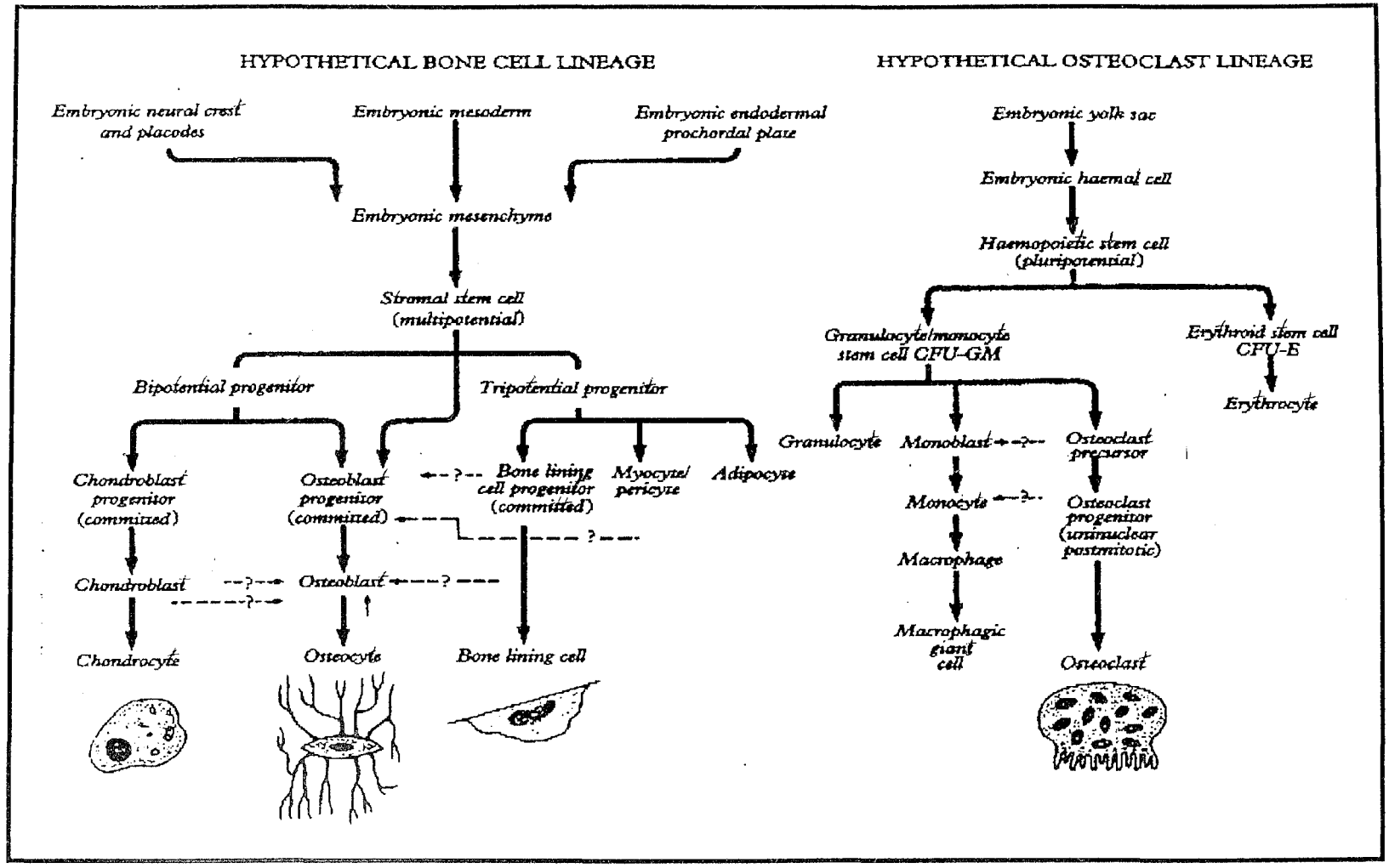

Figure 3.3 Hypothetical bone cell lineage[31].

formation in balance [35]. Removal and deposition of bone occur most prominently both along the outer surface of the bone underlying the periosteum and on the inner surface of the marrow cavity.

Osteoblasts, responsible for bone formation, are small cuboid cells, containing single nucleus, making type 1 collagen, synthesizing osteocalcin, osteonectin, etc., secreting alkaline phosphatase, and with receptor sites for PTH, and 1,25-dihydroxy Vitamin D. Mature osteoblasts in their final stage of development, contained in their lacunae are named as osteocytes. Inactivated osteoblasts make the lining cells, covering the bone surface, regulating water-mineral exchange and preserving the calcium balance [31]. Osteoclasts, responsible for bone resorption, are big cells, with many nuclei, non-cuboidal at the point of attachment, producing enzymes and H^+, degrading the organic matrix, releasing calcium and phosphorus, and do not have receptor sites for PTH and 1, 25-dihydroxy Vitamin D. Osteoclasts, the main protagonists involved in bone resorption mechanisms, are generally considered to be of haematopoietic origin [19] (see Figure 3.3), although the exact nature of the primary osteoclastic stem cells is still unknown. In vitro cellular models developed to study the different events of osteoclastic differentiation have revealed that not only several cell types (osteoblasts, monocytes, lymphocytes, etc.) but also many soluble factors (cytokines, hormones, vitamins, ions, etc.) and extracellular matrix elements (osteopontin, osteocalcin, etc.) are involved in osteoclastic differentiation and activation. Isolated osteoclasts are inactive.

Calcified bone is formed by a process known as ossification, which occurs in two different ways: intramembraneous bone formation and endochondral bone formation. Intramembraneous bone formation involves direct calcification of the organic bone matrix; endochondreal bone formation involves the replacement of a cartilaginous structure by calcified bone.

Intramembraneous bone formation begins with the differentiation of mesenchymal connective tissue cells, osteoblasts, which synthesize collagen fibers and an organic ground

substance and surround themselves with this nonmineralized matrix, known as osteoid. As the osteoid becomes mineralized, small islands of bone are formed, each surrounded by a single layer of osteoblasts. Adjacent spicules then fuse at various points to form a spongelike structure. As the process continues, some of the osteoblasts are trapped within the mineralized matrix and become osteocytes. Mesenchymal tissue trapped within the spaces of the cancellous bone eventually gives rise to the hematopoietic tissue of the bone marrow. The layer of mesenchymal tissue surrounding the developing bone becomes periosteum; from this periosteal sheath further osteoblasts arise and add new concentric layers of ossified bone to the growing network of spicules. As the bone matures, the spaces between the spongy-bone tissue near the periosteum become filled with calcified bone tissue to form compact bone.

Endochondral bone formation begins with the embryonic differentiation of mesenchymal cells into chondroblasts, which deposit a matrix of cartilage in the shape of the developing bone. The outer sheath of cartilage forming cells, the perichondrium, transforms into a sheath of bone-forming cells, the periosteum. This occurs initially around the mid-region of the bone shaft. At the inner surface of the periosteum, adjacent to the cartilaginous bone, osteoblasts begin to lay down a mineralized matrix of bone in a manner resembling the process of intramembraneous bone formation. At the end of this stage, the developing bone consists of a mineralized shaft with two large masses of cartilage at the epiphyses. Osteoblasts then invade the epiphyses to form secondary centers of ossification at the two ends of the bone. The formation of these secondary centers of ossification begins in different bones sometime between birth and the first three years of life. Between the primary ossification center along the shaft of the bone and the two secondary ossification centers at the epiphyses are layers of growing cartilage. In these regions, known as the epiphyseal plates, the growth of cartilage approximately keeps pace with the rate at which it is being replaced by mineralized bone.

Four zones exist within the epiphyseal plate. Resting cartilage constitutes the most distal zone and contains chondrocytes distributed at random throughout its matrix. Next is the zone of chondrocyte multiplication, which is the major area for new cartilage deposition; in this zone the cells become arranged in rows parallel to the long axis of the bone. In the third

zone, the zone of chondrocyte hypertrophy, the cells become enlarged and show signs of beginning disintegration. In the last zone, the zone of cartilage calcification, mineralized bone replaces the disintegrating cartilage; this zone, which is closest to the diaphysis, receives a rich blood supply from the underlying marrow. By this continuous process of cartilaginous growth and replacement by mineralized bone, the ends of the long bone are able to elongate during the years of growth. Eventually, the epiphyseal plates at the ends of the bone become completely replaced by bone tissue and further lengthening of the bone ceases. This occurs at various ages in the different bones but is usually complete in all the long bones by 20 years of age.

3.4 Fracture Healing and Callus Remodeling

When a bone is cracked or broken, the repair process is initiated by the migration of blood vessels and connective tissue from the periosteum into the region of the break. This dense fibrous tissue fills in the break and forms a temporary union, or callus. The cells near the broken edges differentiate into osteoblasts; those further away become chondroblasts and begin to deposit cartilage between the broken surfaces of the bone. This cartilage is slowly replaced by mineralized bone tissue, thereby completing the repair.

Two tissues provide the cells responsible for the healing of a typical fracture: the periosteum and the marrow of the injured bone. The periosteum has a fibrous outer layer and a highly cellular cambium or inner layer. The osteoblasts of the periosteum, which produce lamellar bone at a slow pace, are stimulated at slight trauma to produce more osteoblasts, which make woven bone in a short amount time. In the case of a fracture, the periosteal woven bone takes the form of trabeculae, which arch over the fracture line and fuse to bridge the gap and make what is known as the periosteal callus.

The endosteal surfaces of bones are not actually covered by a membrane. Instead they are lined with bone lining cells, this is true whether or not the endosteal space contains trabecular bone. In places, the endosteal surface may be experiencing ordinary modeling, but most of the adult endosteal surface is quiescent. The bone lining cells may be stimulated to

Boğazici Universitesi Kütüphanesi

initiate bone remodeling by various factors, including mechanical ones, but such remodeling does not play a role in the initial fracture healing response. Instead, trauma to the marrow stimulates the formation of the medullary version of the periosteal callus. It has been shown that even without fracture of the cortex, mechanical disruption of the marrow activates the differentiation of osteoblasts and the formation of woven bone within the medullary canal. This bone formation is a prerequisite to the regeneration of the hematopoietic function of the marrow and so serves a dual role when fracture occurs. The periosteal callus tends to be more obvious, but the medullary callus is usually considered to be more important in achieving initial union. Obviously, the jagged ends of the broken bone as well as other trauma to the fracture site, can be expected to break many blood vessels. The resulting hematoma was once thought to be the primary source of the cells responsible for fracture healing. It is now thought that most of these cells come from the marrow and periosteum.

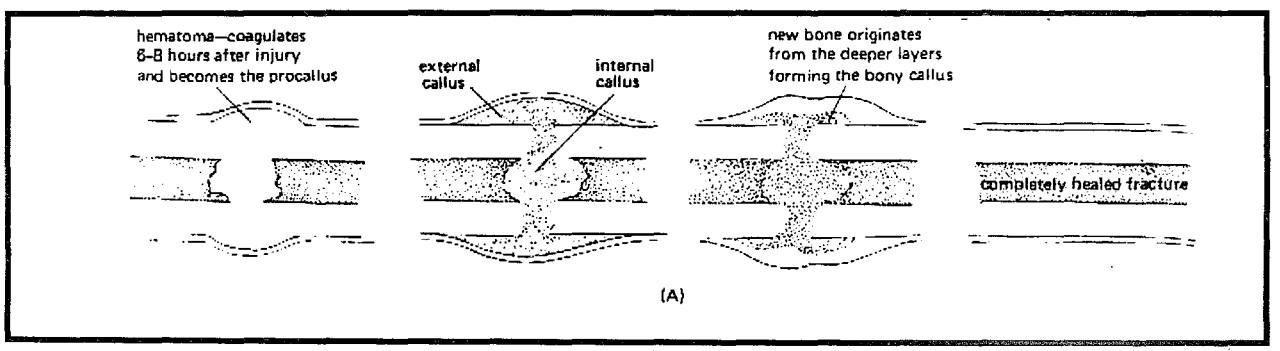

Figure 3.4 Development of fracture callus[36].

3.4.1 Phases of Bone Healing

Healing of a fracture may be divided into inflammatory, reparative, and remodeling phases. These phases are pictured in Figure 3.4 and are explained below.

3.4.1.1 Inflammatory Phase The initial phase serves to immobilize the fractured bone and activate the cells responsible for repair. Immobilization is promoted by pain and by swelling, which in many cases serves to hydrostatically split the fracture. In addition to hematoma formation, this phase is characterized by vasodilation, serum exudation, and infiltration by inflammatory cells. It lasts three to seven days. It is important to realize that fracture repair is not accomplished by existing osteoblasts and chondroblasts but depends on the creation of an entirely new work force of cells from a relatively small population of stem cells. The mobilization of this work force requires a variety of chemical mediators and ancillary cell types that are poorly understood. It involves as series of biological cascades, where each step is predicated on what happened earlier. A mistake in this process may lead to a wrong turn. It follows that many if not most non-unions or delayed unions are caused by a defect in the initial mobilization of the repair process, and once the problem becomes apparent, there is no way to correct it by manipulating the current group of cells. This is consistent with the fact that one of the most effective treatments for nonunions is to replace the tissues in the fracture site with a bone graft, which essentially initiates an entirely new repair process. Alternatively, electrical signals may be able to start a new cascade.

3.4.1.2 Reparative Phase In this phase of healing, which lasts about one month, the periosteal and medullary calluses are formed by osteoblasts from the periosteum and marrow. The stem cells for medullary osteoblasts are thought to be multipotential mesenchymal cells in the marrow stroma. These cells are also stem cells for fibroblasts, chondroblasts and some marrow cells. Mesenchymal cell proliferation and differentiation are accompanied by intense vascular proliferation. The resulting osteoblasts produce woven bone at a high rate. The fracture site exhibits some degree of endochondral ossification as well as direct bone formation by osteoblasts. This is thought to be related to inadequate blood supply in some

portions of the fracture region. In the absence of adequate vascularization, stem cells are thought to differentiate into chondroblasts rather than osteoblasts. An important contributing factor to the inadequate vascularization can be insufficient immobilization of fracture fragments. Alternatively, the nature of the stresses at a site within the callus may affect the differentiation pathway. In any event, the chondrogenic regions of the callus, which tend to be near the fracture line, usually calcify and are replaced by lamellar bone, just as the woven bone regions are. If this does not happen, pseudoarthrosis may develop. Regardless of how much of the callus is cartilaginous, it takes a week or two for the woven bone or cartilage to accumulate substantial mineral. This early phase of callus is known as provisional callus. As calcification proceeds, the callus material becomes increasingly rigid, it is then referred to as the bony callus. The rigidity of the callus is enhanced by the fact that it has a larger cross-sectional area (and moment of inertia) than the original bone cortex. This means that even though the material in the bony callus is less rigid and strong than cortical bone, the rigidity and strength of the callus structure can equal or exceed that of the intact bone. When this occurs, bony union has been achieved, completing the reparative phase.

3.4.1.3 Remodeling Phase When bony union has been achieved, the broken bone is approximately as strong as the intact bone was, but often it has greater mass than the original bone, and is therefore less mechanically efficient. Modeling and remodeling of the fracture site gradually restore the original contour and internal structure of the bone (see Figures 3.4 and 3.5), although radiographic evidence of the fracture may persist for many years. As the bone remodels, it is able to maintain its strength with differently oriented material than in the earlier phases of healing, thereby increasing its mechanical efficiency. The medullary and periosteal calluses are removed and the remaining material (woven bone or calcified cartilage) is replaced by secondary lamellar bone (cortical or trabecular, as the site dictates). If the fracture has healed with incorrect angulation, or secondary axial displacement, this may be partially corrected as well, by modeling drifts.

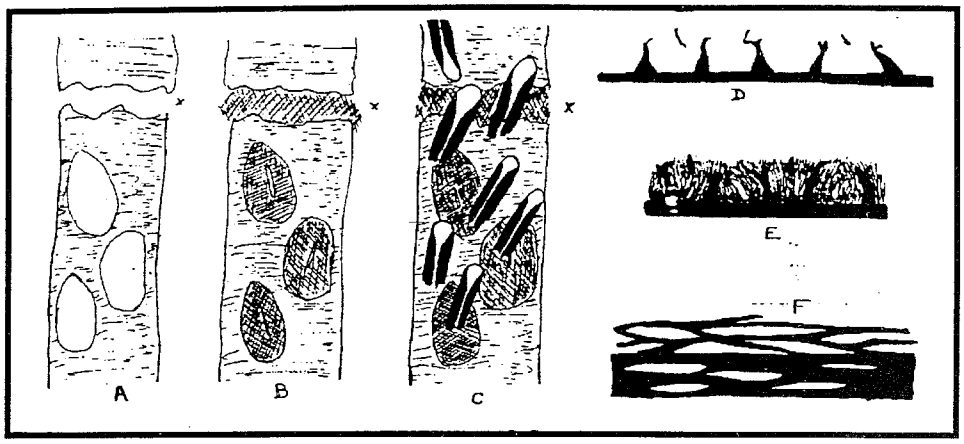

Figure 3.5 Callus remodeling. Osteocytes form the resorption cavities, which extend throughout the bone as well and the mineralizing callus. The resorption cavities are then filled in with new bone[37].

3.4.2. Stability of Fixation

Longer bones are more prone to nonunion than others as the result of excessive motion of the fragments. It seems that the amount of callus is inversely related to the motility of the fragments and that applying some weight on the callus strengthens the callus up to a certain point. Healing of the tightly fixed and closely approximated bone ends occurs by osteonal remodeling across the fracture line, which is named as primary fracture healing. Healing is the fracture healing which has been described in the above section.

As healing occurs intact portions of fractured bone become osteoporotic, which may be due to two factors: (a) during the healing response osteonal BMUs (bone modelling units made up of osteoblasts, osteoclasts and lining cells) form resorption cavities throughout the entire cortex, and (b) as mechanical loading is removed from the fractured bone remodeling is activated. In the case of a well fixed fracture, where load-bearing can be easily resumed, resorption spaces refill and osteopenia is transient. If load-bearing is not resumed, then atrophy persists.

3.4.3 Four Biomechanical Stages

The extent of fracture healing is determined mechanically by testing the healing bone in torsion. In rabbit tibial fractures, four stages of healing have been identified. In stage I, the inflammatory and early reparative (i.e. provisional callus) phases of healing (Days 1-26 in the rabbit tibia), where no stiffness is seen, failure occurs through the original fracture line. In stage II, the middle of the reparative phase when the callus has become bony but still is not so large or calcified as it will become (Days 27-49 in the rabbit tibia), although there is substantial stiffness, failure still occurs through the original fracture line. In stage III, (Days 49-56 in the rabbit tibia), there is no further increase in stiffness, but failure is now partially through the original fracture line and partially through intact bone. In stage IV, after day 56 in the rabbit tibia, failure occurs through the intact bone rather than the callus at the fracture site.

Stages III and IV correspond to the later portion of the reparative phase and the early remodeling phase, when the full bony callus exists but its mineral content and the strength are still increasing. Another interesting observation from these mechanical studies of healing fractures is that there is typically a slight reduction in the strength of the fracture callus during stage IV of healing. It is reasonable to think that this corresponds to the beginning of the remodeling phase, when the resorptive portion of BMU activity has begun, but substantial refilling of the osteonal cavities has not occurred yet.

3.5 Mechanotransduction in Bone

Mechanotransduction plays a crucial role in the physiology of many tissues including bone. Mechanical loading can inhibit bone resorption and increase bone formation in vivo. In bone, the process of mechanotransduction can be divided into four distinct steps: (1) mechanocoupling, (2) biochemical coupling, (3) transmission of signal, and (4) effector cell response.

In mechanocoupling, in vivo mechanical loads cause deformations in bone, which stretch the bone cells within and lining the bone matrix and create fluid movement within the canaliculae. Dynamic loading, which is associated with extracellular fluid flow and the creation of streaming potentials within bone, is most effective for stimulating new bone formation in vivo. Cells, when subjected to hydrostatic micropressures of 20 kPa or less demonstrate a perturbation in growth and/or metabolism. The general conclusion is that cells probably respond to micro-pressures through a mechanical process. Differential compression of cellular structures is likely to cause shear and strain, leading to changes in enzyme and/or ion channel activity [38].

Bone cells in vitro produce second messengers when exposed to fluid flow or mechanical stretch. In biochemical coupling, the possible mechanisms for the coupling of cellular level mechanical signals into intracellular biochemical signals include force transduction through the integrin-cytoskeleton-nuclear matrix structure, stretch-activated cation channels within the cell membrane [39], voltage operated calcium channels, VOCCs, G protein-dependent pathways, and linkage between the cytoskeleton and the phospholipase C or phospholipase A pathways [40].

The tight interaction of each of these pathways would suggest that the entire cell is a mechanosensor and there are many different pathways available for the transduction of a mechanical signal. In the transmission of signal, osteoblasts, osteocytes, and bone lining cells may act as sensors of mechanical signals and may communicate the signal through cell processes connected by gap junctions. These cells also produce paracrine factors that may signal osteoprogenitors to differentiate into osteoblasts and attach to the bone surface. Insulin-like growth factors and prostaglandins are possible candidates for intermediaries in signal transduction. A number of secondary messenger pathways have been implicated in load transduction by bone cells, and many of these pathways are similar to those proposed for other load-responsive cell types. It appears that load transduction involves interaction between several messenger pathways, rather than one specific switch [39]. Interaction between these pathways may result in a cascade of responses that promote and maintain bone cell activity in

remodeling of bone. The involvement of calcium channels in the immediate load response and the modulation of intracellular calcium may be used as an early signal [40].

In the effector cell response, the effects of mechanical loading are dependent upon the magnitude, duration, and rate of the applied load. Longer duration, lower amplitude loading has the same effect on bone formation as loads with short duration and high amplitude. Loading must be cyclic to stimulate new bone formation. Aging greatly reduces the osteogenic effects of mechanical loading in vivo. Also, some hormones may interact with local mechanical signals to change the sensitivity of the sensor or effector cells to mechanical loading.

A biomechanical approach to bone formation is Frost and Jee's Mechanostat Theory, strain adaptive remodeling of bone [41,42] which distinguishes between modeling and remodeling processes, lamellar and woven bone formation, mechanical usage windows for activation and disorders of bone and mineral metabolism (Figure 3.6). Differences in patterns of bone formation and different amount of porosity in the compression and tension cortices of bones may also be explained by this theory. The high number of cracks and associated resorption sites are higher in the tensile and disuse areas [44] as well as the number of osteons and secondary osteons [45]. In vivo studies show that static loads do not play a role in mechanotransduction and that bone formation is threshold-driven and dependent on strain rate, amplitude and duration of loading. There is also indirect evidence that mechanical strains cause interstitial fluid flow, which activates the bone cell response. Strain rate may determine the vigor of osteoblastic activity and the regularity of loading bouts determines osteoblast recruitment [43].

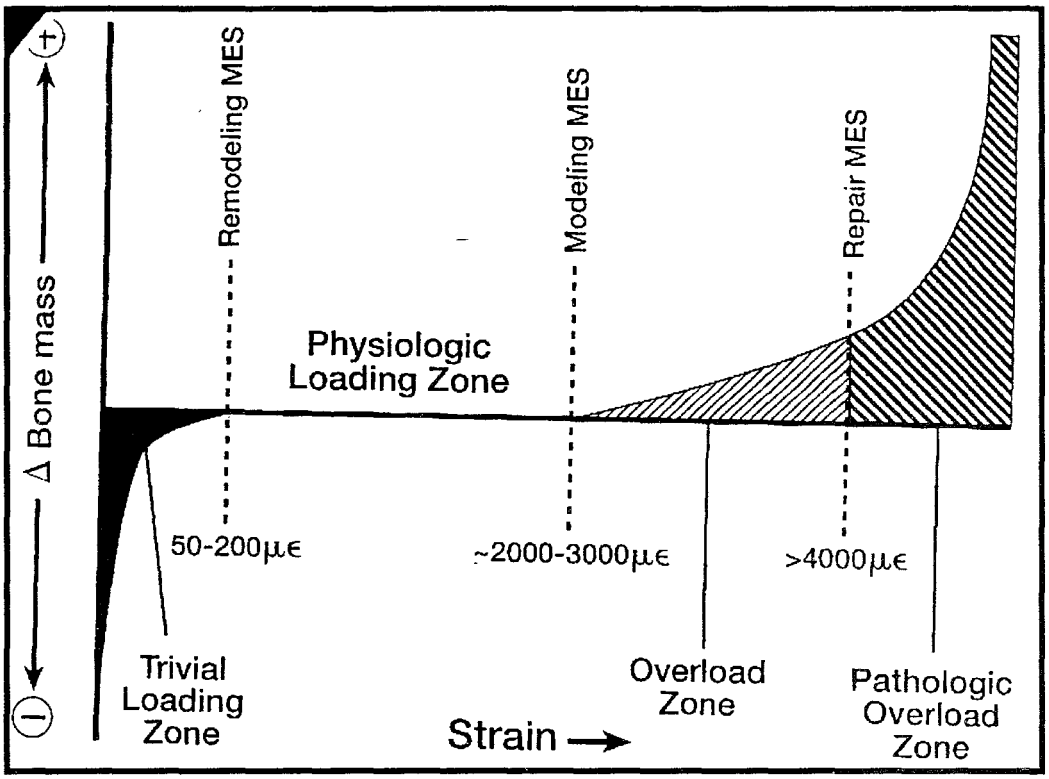

Figure 3.6 Strain adaptive remodeling of bone. In the trivial loading zone, osteocytes are activated and preosteocytes proliferate, with increased remodeling and insufficient bone formation. In the physiologic loading zone, there is subtle modulation of osteocyte and osteoblast activity during the remodeling cycle and on modeling surfaces during growth. Modeling surfaces are quiescent in adult. In mild overuse window, there is increased preosteoblast proliferation and recruitment of osteoblasts from preosteoblasts and activation of bone formation on previously quiescent surfaces[45].

Complementing Frost's theory is that of Turner's [43,46], which argues that while fracture callus and woven bone formation are regulated epigenetically, involving positive feedback loops and promoting differentiation as the elements of a system have to choose between the two extreme levels of attractors, the lamellar bone formation may be regulated homeostatically, through the involvement of negative feedback loops, as stated by Frost and Jee.

4. EXPERIMENTAL STUDY

4.1 Osteotomies

Osteotomies were carried out at the Experimental Animals Laboratory of İstanbul University, Cerrahpaşa Medical School, after permission was granted from the Ethic Committee of the Istanbul University. 20 male, 10 week-old, white Wistar rats, weighing from 131 gr. to 160 gr., were used. Animals were anesthesized, using 3 mg/kg intramuscular injections of xylazine hydrochloride (Rompun 23.32 mg/ml, Bayer Turk, İstanbul, Turkey) and 10 mg/kg ketamine hydrochloride (Ketalar 50 mg/ml, Eczacıbaşı, Istanbul, Turkey). Hindlimbs of the animals were shaved and washed with polyvinylpyrolidon (Poviod, Saba, Istanbul, Turkey). A 2 cm incision was made over the femur and the muscles were reflected. Using a mini-saw, a transverse defect was created in the midshaft of the femur. The periosteum was preserved and a 1.0 mm thick Kirschner wire was inserted through the medullary canal, extending proximally and distally. Following wound irrigation with saline solution, the overlying tissues were repaired using 4-0 synthetic absorbable lactomer 9-1 sutures (Polysorb, USSC, US). As a prophylactic antibiotic, 10 mg/kg/day of cefazolin sodium (Cefazin injectable, IM, 1 gr/mg, Bilim İlaç A.Ş., İstanbul, Turkey) was given intramuscularly after the operation. No complications occurred during and after the operation and all of the animals survived without infections. After the operation, animals were not immobilized (according to Schleberger and Senge [15]).

4.2 Extracorporeal Shock Wave Treatment

On the 20^{th} day, animals were divided into two groups of ten animals each and were treated with ESW. Animals were anesthesized with 3 mg/kg intramuscular injections of xylazine hydrochloride (Rompun 23.32 mg/ml, Bayer Turk, İstanbul, Turkey) and 10 mg/kg ketamine hydrochloride (Ketalar 50 mg/ml, Eczacıbaşı, Istanbul, Turkey). The right femurs of

animals in the first group were exposed to 1500 shockwaves/treatment at a generating voltage of 10 kV (frequency = 120, power 10.4 W) using a hydraulic lithotriptor (PCK Medical Systems, Stonelith-Litho3pter, Ankara, Turkey) (Figure 2.2). Output of the shockwave generator was determined by the generator voltage setting. The shockwaves were focused on the osteotomies radiologically, using a biplanar intersecting X-Ray system with image intensifier chain and a television monitor for target imaging. In order to attain perfect coupling, ultrasound gel was used and target location was rechecked several times during the course of treatment. The untreated left femurs were used as controls. One animal from this group did not receive ESW treatment due to diarrhea. The right femurs of animals in the second group were exposed to 500 shockwaves/treatment at a generating voltage of 10 kV (frequency = 120, power 10.4 W) using the above-mentioned hydraulic lithotriptor. The untreated left femurs were used as controls. One animal from this group did not receive ESW treatment due to high tolerance to anesthetics.

After ESWT, the animals were not immobilized. During the course of the experiment, four animals from the first group and two animals from the second group died due to diarrhea. The remaining five animals from the first group and the seven animals from the second group lived till the termination of the experiment.

The experiment was terminated on day 64, forty-four days after ESW treatment. Animals were sacrificed by ether intoxification. Bones were excised; muscle and soft tissues around the bones were removed, with only the callus remaining. The femurs were fixed in 10% formalin solution for five hours and then preserved in a 50% v/v ethanol solution in plastic centrifuge tubes. During the following examinations bones were kept in plastic tubes as much as possible to prevent drying.

4.3 Radiological Examination

4.3.1 X-Ray Filming

Topographic X-Ray films of bones were taken and used to determine the stage of bone healing. Three independent examiners, who were blind to the experiment, carried out radiological scoring of early, middle and late phases of bone healing. Scores on periosteal reaction, quality of union, and bone remodeling were summed. The sums were analyzed using Student's t-test to find significance of results between and within the groups [46]. Bone healing of the femurs was blindly quantified by scoring on the healing parameters using a system modified by An et al. [48] as listed in Table 4.1.

Table 4.1.
Radiographic scoring system for bone healing[48].

Categories	Scores
Periosteal Reaction	
Full (across the defect)	3
Moderate	2
Mild	1
None	0
Bone Union	
Union	3
Moderate Bridge (>50 %)	2
Mild Bridge (<50 %)	1
Nonunion	0
Remodeling	
Full Remodeling Cortex	2
Intramedullary Canal	1
No Remodeling	0
Maximum Total Score	**8**

4.3.2 Computerized Tomography (CT)

Callus size and density were measured using a high resolution CT (Siemens, Somatom AR Star). Contiguous 1.0 mm CT slices were taken from proximal to distal at a slice thickness of 1.0 mm. Measurements were carried out throughout the medullary canal. The periphery of callus was drawn manually, giving us both the callus area in square milimeters and the average value of image pixel, which is the mean value of all the pixels within the region of interest (ROI), in Hounsfield unit scale, with values ranging from 0 (for air) to 4095. Callus area and average value of image pixel analyses between and within groups were performed using Student's t-test.

4.3.3 Dual Energy X-Ray Absorptiometry (DEXA)

Bone density was measured using Dual Energy X-Ray Absorptiometry (Lunar, DPX-IQ, U.S.)(see Figure 4.1). Manual analysis was used and the measurements taken from the region of interest were recorded in g/cm^2. Pixel spacing was 0.5 mm. x 0.5 mm., the scan width, 3 cm., and the scan speed 10 mm/sec. The start point of the scan was located above the

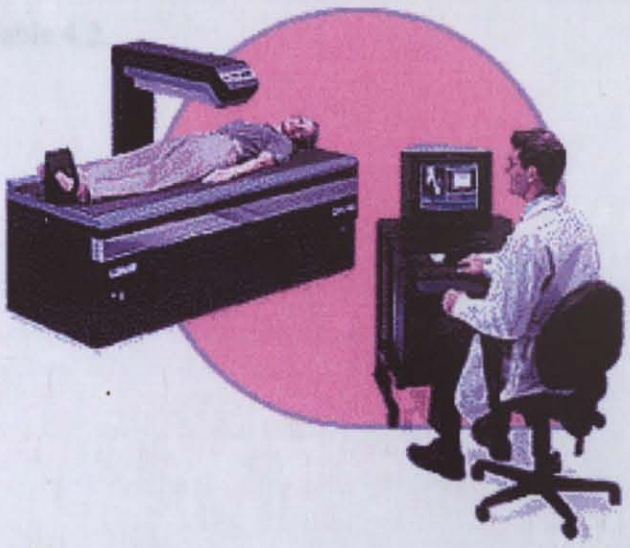

Figure 4.1 DEXA Lunar DPX-IQ bone densitometer [49].

proximal end of the femur and the end point below the distal end of the femor, so that the scanner arm moved along the long axis of the femoral shaft allowing evaluation of femur length. All DEXA scans and measurements were done by the same operator. All of the specimen were laid on their posterior side in a water bath. Bone mineral content (BMC) and bone mineral density (BMD) were determined from the region of interest (ROI), which is the entire body of the femur. The entire body of the femur, outlined by the operator, gave us the area of femur needed to determine the BMD.

4.4 Histological Studies

In order to evaluate the stage of bone healing, histological methods were used. Minerals in the specimen were removed by placing them in decalcification solution. The organic component of the bones were embedded in paraffin and thin sectioned longitudinally. These sections were then stained with hematoxylin and eosin dyes to visualize the different tissue and cell types allowing an evaluation of the stage of bone formation. Stage of bone healing was determined according to certain histological parameters modified by An et al. [45]. The parameters for histomorphometry, original and new bone area, chondral tissue, fibrocartilage, fibrous vascular tissue (marrow), callus formation, bone union, cortex remodeling, are listed in Table 4.2.

Table 4.2.
Histological scoring system for bone healing[48].

Categories	Scores
Callus Formation	
Full (across the defect)	3
Moderate	2
Mild	1
None	0
Bone Union	
Full Bone Bridge (Union)	3
Moderate Bridge (> 50 %)	2
Mild Bridge (< 50 %)	1
No New Bone in the Fracture Line (Nonunion)	0
Marrow Changes	
Adult Type Fatty Marrow	4
2/3 Replaced by New Tissue	3
1/3 Replaced by New Tissue	2
Fibrous Tissue	1
Red	0
Cortex Remodeling	
Full Remodeling Cortex	2
Intramedullary Canal	1
No Remodeling	0
Maximum Total Score	12

5. RESULTS

5.1 Macroscopic Examination of Bones

Bones were macroscopically examined; physical properties of both rats and femurs, the union angles, callus sizes, and the unions and nonunions were recorded.

Table 5.1.
Macroscopic examination of Group I - 1500 sw/treatment.

Animal Number / Femur	Animal Size	Femur Length	Union Angle	Callus Size	Presence of Union
# 1 Right Femur	(1)	2.9 cm	0°*	Small	Nonunion
# 1 Left Femur	(1)	2.5 cm	150°	Large	Nonunion
# 2 Right Femur	(1)	2.6 cm	180°	Large	Nonunion
# 2 Left Femur	(1)	2.5 cm	150°	Large	Nonunion
# 3 Right Femur	(2)	3.0 cm	140°	Large	Nonunion
# 3 Left Femur	(2)	2.5 cm	180°	Medium	Nonunion
# 4 Right Femur	(2)	2.5 cm	110°	Large	Nonunion
# 4 Left Femur	(2)	3.0 cm	160°	Medium	Union
# 5 Right Femur	(3)	3.6 cm	180°	Small	Union
# 5 Left Femur	(3)	3.7 cm	180°	Small	Union

(1) small animals weighing between 130-160 gr.
(2) medium size animals, weighing between 160-200 gr.
(3) large animals, weighing more than 200 gr.
*During excision of femur, bone fragments detached from each other.

In the first group, listed in Table 5.1, there were seven nonunions and three unions. Only four of the femurs did not have secondary axial displacements. Callus size in nonunions varied from medium to large; while in the unions it varied from small to medium. The fifth animal in this group was the largest in size of both groups, and had the longest femur. Macroscopically, there is indication that callus size may vary with secondary axial displacement and the presence of a nonunion.

Table 5.2.
Macroscopic examination of Group II - 500 sw/treatment.

Animal Number/ Femur	Animal Size	Femur Length	Union Angle	Callus Size	Presence of Union
# 1 Right Femur	(2)	3.1 cm	180°	Small	Union
# 1 Left Femur	(2)	3.1 cm	180°	Small	Union
# 2 Right Femur	(1)	3.2 cm	180°	Small	Union
# 2 Left Femur	(1)	3.1 cm	180°	Small	Union
# 3 Right Femur	(2)	2.8 cm	180°	Medium	Union
# 3 Left Femur	(2)	2.8 cm	180°	Small	Union
# 4 Right Femur	(2)	2.8 cm	110°	Medium	Nonunion
# 4 Left Femur	(2)	2.9 cm	180°	Small	Union
# 5 Right Femur	(2)	2.4 cm	100°	Small	Nonunion
# 5 Left Femur	(2)	3.0 cm	180°	Small	Union
# 6 Right Femur	(1)	3.0 cm	180°	Medium	Union
# 6 Left Femur	(1)	3.0 cm	180°	Medium	Union
# 7 Right Femur	(3)	3.6 cm	180°	Small	Union
# 7 Left Femur	(3)	3.3 cm	160°	Medium	Union

In the second group, listed in Table 5.2, there were two nonunions and twelve unions. The two nonunions had secondary axial displacements, and below the average femur length (ave. 2.99 cm). Callus size in this group varied from small to medium.

Table 5.3.
Macroscopic examination of right and left femurs.

Group	Union	Nonunion
I (1500 sw)	(3) 1 right, 2 left	(7) 4 right, 3 left
II (500 sw)	(12) 5 right, 7 left	(2) 2 right

The ultimate criteria of bone healing is the presence of a union. Results of macroscopic examination of bone union, listed in Table 5.3, show that in the first group, the total number of nonunions and the number of nonunions in the right femurs is higher than the second group. On the contrary, the second group has a higher number of unions than nonunions. The two nonunions are in the right femurs.

5.2 Radiological Assessment

5.2.1 Topographic X-Ray Analysis

Radiography is the basic method used in the evaluation of bone healing. Right and left femurs, belonging to the same animal, were placed side by side, in their anatomic directions, and a single 22 kVP, 22.0 MAS X-Ray image of the bones was taken (see Figure 5.1). The radiological examination results, listed in Table 5.4, were in complete agreement with the macroscopic examination results listed in Table 5.3. X-Ray film of bones were assessed on the quality of bone healing by three independent orthopedists blind to the experiment. The radiological scores given by the orthopedists were added and averaged. As expected, the femurs with nonunions had lower (below 3) radiological scores than those with unions and most of the nonunions were at the periosteal reaction stage (listed in Tables 5.5 and 5.6).

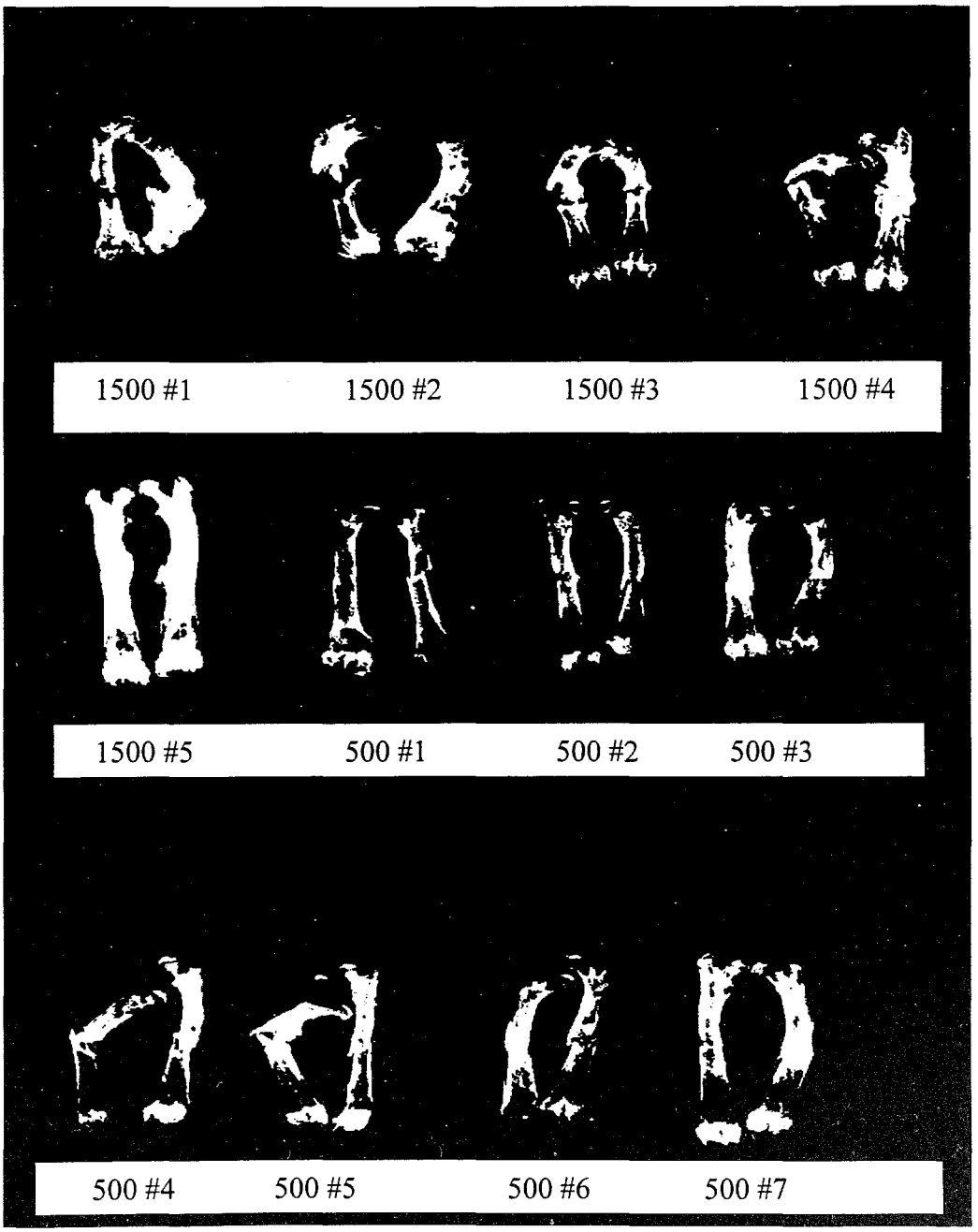

Figure 5.1 X-Ray film of both groups of bones.

Table 5.4.
Radiological examination of right and left femur.

Group	Union	Nonunion
I (1500 sw)	(3) 1 right, 2 left	(7) 4 right, 3 left
II (500 sw)	(12) 5 right, 7 left	(2) 2 right

Table 5.5.
Radiological scores of Group I.

Animal/ Femur	Periosteal Reaction	Quality of Union	Bone Remodeling	Total Score
1 / Right Femur	0	0	0	0
1 / Left Femur	0.67	1.33	0.67	2.67
2 / Right Femur	0	0	0	0
2 / Left Femur	2	0.67	0	2.67
3 / Right Femur	1.33	0	0	1.33
3 / Left Femur	1	0	0	1
4 / Right Femur	0	0	0	0
4 / Left Femur	2	1.67	0.67	4.34
5 / Right Femur	3	3	2.33	8.33
5 / Left Femur	3	3	2.33	8.33
Right Femur	**4.33**	**3**	**2.33**	**9.66**
Left Femur	**8.67**	**6.67**	**3.67**	**19.01**
Total	**13**	**9.67**	**6**	**28.67**
Total Average	**1.3**	**0.967**	**0.6**	**2.867**

Table 5.6.
Radiological scores of Group II.

Animal/ Femur	Periosteal Reaction	Quality of Union	Bone Remodeling	Total Score
1 / Right Femur	3	3	1.67	7.67
1 / Left Femur	2.33	2.33	0.67	5.67
2 / Right Femur	2.67	1.67	0.67	5
2 / Left Femur	2.67	2.67	2	7.3
3 / Right Femur	3	3	1.67	7.67
3 / Left Femur	3	2.33	0.67	6
4 / Right Femur	1	0	0	1
4 / Left Femur	3	3	1.33	7.33
5 / Right Femur	1	0	0	1
5 / Left Femur	3	3	1.33	7.33
6 / Right Femur	3	2.33	0.67	6
6 / Left Femur	3	2.67	1.33	7
7 / Right Femur	2.67	2	0.67	5.33
7 / Left Femur	3	3	1.33	7.33
Right Femur	**16.34**	**12**	**5.35**	**33.69**
Left Femur	**20**	**19**	**8.66**	**47.66**
Total	**36.34**	**31**	**14.01**	**81.35**
Total Average	**2.59**	**2.21**	**1.0**	**5.81**

5.2.2 Computerized Tomographic Analysis

Callus size and properties were examined using high resolution CT, giving minimum and maximum average density of image pixel and callus area in squared milimeters (listed in Table 5.7).

Table 5.7.
Summary of callus density and area.

	Min. and Max. Average Density of Image Pixel	Total Callus Area (mm^2)
Group I - Right Femurs	-170 to 400 (sd. 403)	5.72
Group I - Left Femurs	122 to 560 (sd. 309)	6.6
Group II – Right Femurs	-80 to 158 (sd. 168)	1.34
Group II – Left Femurs	-153 to 168 (sd. 226)	0.57

The Group I average densities of image pixel for the right and left femurs have a greater standard deviation than Group II. The average densities of Group I are higher than that of Group II. Callus area of Group I is greater than that of Group II. Minimum and maximum average density of image pixel, the standard deviation and callus area of Group I are higher than those of Group II. In Group I, the left femurs have a slightly greater average density of image pixel and callus area than the right femurs. In Group II, the right femurs have a slightly larger callus area than the left femurs.

5.2.3 DEXA - Dual Energy X-Ray Absorptiometric Analysis

The Dual-Energy X-Ray Absorptiometry results are listed below, in Tables 5.8 and 5.9. The DEXA images are given in Figures 5.2-5.4.

Table 5.8.
DEXA values of animals in Group I.

	Right Femur			Left Femur		
Animal #	BMC (gr.)	Area (cm^2)	BMD (gr/cm^2.)	BMC (gr.)	Area (cm^2)	BMD (gr/cm^2.)
1	NA	NA	NA	NA	NA	NA
2	0.086	1.443	0.059	0.114	1.552	0.075
3	0.101	1.407	0.072	0.073	1.362	0.053
4	0.084	1.531	0.055	0.183	1.691	0.108
5	0.254	2.121	0.120	0.259	2.120	0.122
Average	0.131	NA	0.076	0.157	NA	0.089

Table 5.9.
DEXA values of animals in Group II.

	Right Femur			Left Femur		
Animal #	BMC (gr.)	Area (cm^2)	BMD (gr/cm^2.)	BMC (gr.)	Area (cm^2)	BMD (gr/cm^2.)
1	0.145	1.309	0.110	0.098	1.262	0.078
2	0.098	1.339	0.073	0.092	1.301	0.071
3	0.103	1.584	0.065	0.070	1.133	0.062
4	0.070	1.344	0.052	0.113	1.569	0.072
5	0.104	1.404	0.074	0.127	1.581	0.080
6	0.114	1.524	0.075	0.114	1.561	0.073
7	0.165	2.043	0.081	0.190	1.889	0.101
Control # 4	0.127	1.290	0.099	0.127	1.222	0.104
Average	0.114	NA	0.076	0.115	NA	0.076

Due to large variation in bone area, there was an equivalent variation in BMC, not only among the bones from different animals, but also between the femurs of the same animal. In Group I, BMD of the left femurs of all animals except for #3, were greater than the right femurs. In Group II, except for animals #1, #4 and #7, there was not a great difference in BMD between the right and the left femurs. In animal #1, the BMD of the right femur was greater than the left femur, whereas in #4 and #7 the opposite was true. Although the BMC of the control animal (unoperated, untreated) did not vary at all between femurs, due to the difference in area, BMD of right femur was slightly lower than that of left femur.

Figure 5.2 DEXA image of femur pairs #2-5, Group I, right and left femurs respectively.

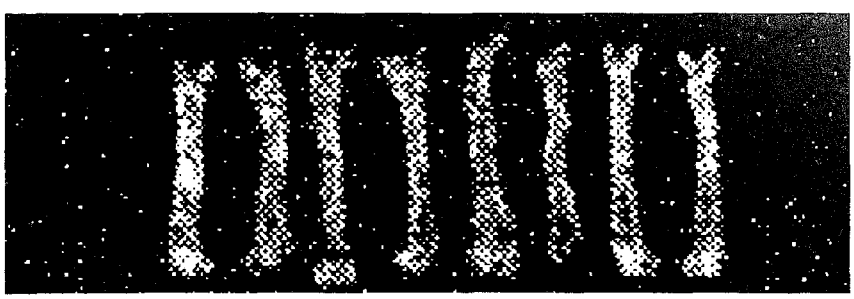

Figure 5.3 DEXA image of femur pairs #1-3, Group II, and unosteotomized control, right and left femurs respectively.

Figure 5.4 DEXA image of femur pairs #7-4, Group II, right and left femurs respectively.

5.3 Histological Analysis

Histological studies were performed on femurs in order to determine the stage of bone healing that was attained. The histological images were examined by a pathologist and bone healing was quantified by scoring on the histological parameters (see Table 4.2), using a system modified by An et al. [48], on callus formation, bone union, marrow changes and cortex remodeling. Tables 5.10 and 5.11 list the results of histological scoring.

Table 5.10.
Histological scores for Group I*.

Animal No. Femur	Callus Formation	Bone Union	Marrow Changes	Cortex Remodeling	Total Score
#1 Right Femur	2	0	1	0	3
#1 Left Femur	3	0	1	0	4
#2 Right Femur	3	0	1	0	4
#2 Left Femur	3	0	1	0	4
#3 Right Femur	3	0	1	0	4
#3 Left Femur	3	0	1	0	4
#4 Right Femur	3	0	1	0	4
#5 Right Femur	3	1	1	0	5
Right Femur Total	**14**	**1**	**5**	**0**	**20**
Left Femur Total	**9**	**0**	**3**	**0**	**12**
Both Femurs Total	**23**	**1**	**8**	**1**	**32**
Femurs Average	**2.87**	**0.12**	**1**	**0.12**	**4.0**

*Only the right femurs of animals #4 and #5 have been studied.

In Group I, despite a fully developed callus formation; none of the tested bones had unions, except for the right femur of animal #5, which had a mild bridge of <50%. The marrow changes were limited to formation of fibrous tissue. In none of the bones, bone healing had advanced to the stage of cortex remodeling and attainment of a defined intramedullary canal.

Table 5.11.
Histological scores for Group II.

Animal No. Femur	Callus Formation	Bone Union	Marrow Changes	Cortex Remodeling	Total Score
# 1 Right Femur	NA	NA	NA	NA	NA
# 1 Left Femur	NA	NA	NA	NA	NA
# 2 Right Femur	3	2	2	0	7
# 2 Left Femur	3	3	3	0	9
# 3 Right Femur	3	2	1	1	7
# 3 Left Femur	3	3	1	0	7
# 4 Right Femur	3	0	1	0	4
# 4 Left Femur	3	3	2	0	8
# 5 Right Femur	3	0	1	0	4
# 5 Left Femur	3	3	1	1	8
# 6 Right Femur	3	0	1	0	4
# 6 Left Femur	3	3	3	1	9
# 7 Right Femur	3	3	4	1	11
# 7 Left Femur	3	3	3	2	11
Right Femurs Total	**18**	**7**	**10**	**2**	**36**
Left Femurs Total	**18**	**18**	**13**	**4**	**52**
Both Femurs Total	**36**	**25**	**23**	**6**	**88**
Both Femurs Average	**3**	**2.08**	**1.91**	**0.5**	**7.33**

In Group II, animal #1 was not studied. Femurs with secondary axial displacements, (animals #4 and #5), as well as the right femur of animal #6 had nonunions. All of the examined femurs had fully developed calluses, while some had unions ranging from a moderate bridge of >50% to a full union. Different levels of changes in bone marrow, varying from one third and two thirds replacement of fibrous tissue by new tissue were observed. Only the right femur of animal #7 contained adult type fatty marrow. Right femurs of animals #3 and #7 and the left femurs of animals #5 and #6 had begun the remodeling of the intramedullary canal. The left femur of animal #7 had a full remodeling cortex.

Table 5.12.
Histological examination of Group I

No.	Right Femur		Left Femur	
	Evaluations	Callus Width	Evaluations	Callus Width
# 1	Pseudoarthrosis Fibrous tissue = 1 mm Chondral ossification area = 1 mm	2.5mm.	Pseudoarthrosis Chondroid metaplasia Synovial tissue Fibrous cartilaginous tissue	9 mm.
# 2	Pseudoarthrosis Osteomyelitis Osteoclastic resorption Granulation tissue	11 mm.	Pseudoarthrosis Suprative osteomyelitis Osteoclastic resorption Granulation tissue	9 mm.
# 3	Pseudoarthrosis Synovial tissue Rice bodies Osteoclastic resorption Granulation tissue (see Figure 5.5)	6 mm.	Pseudoarthrosis Synovial tissue Rice bodies Osteoclastic resorption Granulation tissue	5 mm.
# 4	Pseudoarthrosis Synovial tissue Rice bodies Osteoclastic resorption Granulation tissue	7 mm.	NA	NA
# 5	Union on one side Fibrous tissue between ends (see Figure 5.6)	4 mm.	NA	NA

Evaluations on the histology and callus sizes of femurs of Group I are listed in Table 5.12. Among the femurs in this group, pseudoarthrosis had developed, along with the presence of prominent granulation tissue, fibrous tissue, rice bodies, synovial tissue and osteoclastic resorption. Some femurs displayed chondroid metaplasia. The histological properties did not differ between the right and left femurs. Average callus width in this group (6.68 mm) was greater than that of Group II (3.87 mm).

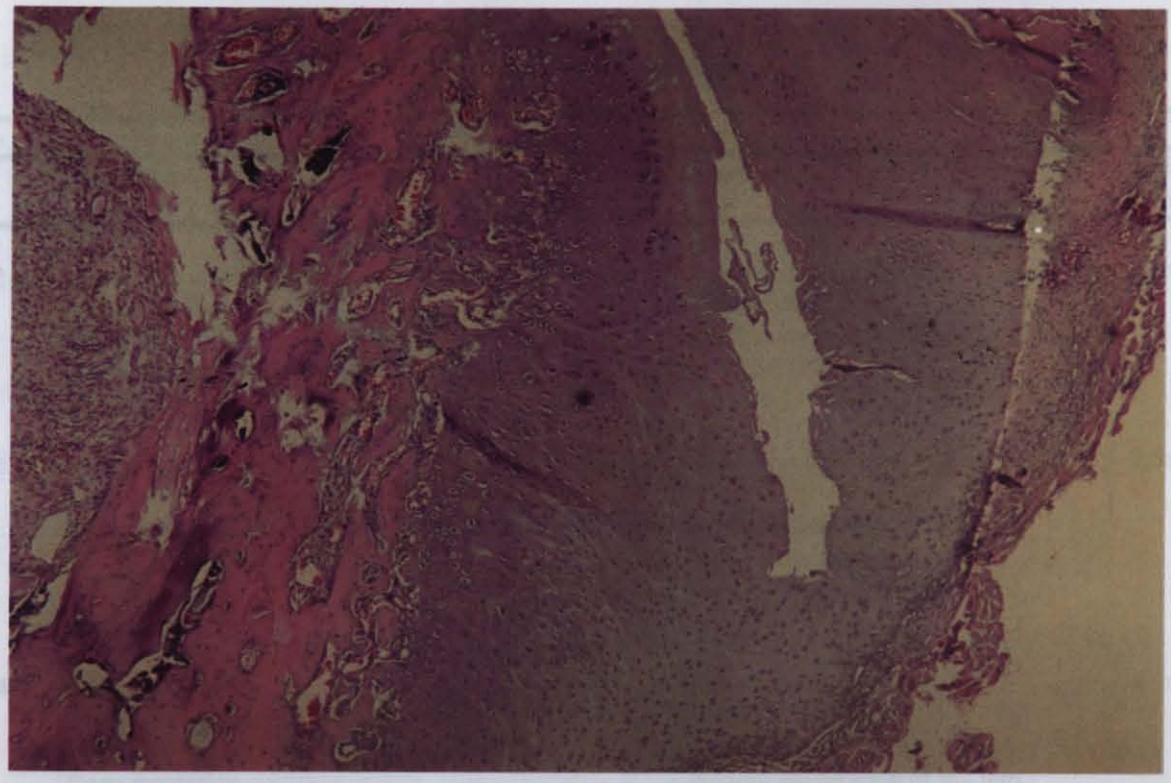

Figure 5.5 Histological section, Group I, animal #3, right femur, H+E stain, 40x, synovial tissue with pseudoarthrosis.

Figure 5.6 Histological section, Group I, animal #5 right femur, H+E stain, 40x, union with a fibrous band between bone ends.

Table 5.13.
Histological examination of Group II

No.	Right Femur		Left Femur	
	Evaluations	Callus Width	Evaluations	Callus Width
# 1	NA	NA	NA	NA
# 2	Unorganized hematoma Fibrous tissue Woven bone Chondral ossification of 1.5 mm. (see Figure 5.7)	5 mm.	Medullary canal = 0.4 mm Fibrous tissue Bone marrow = 1.6 mm (see Figure 5.8)	3 mm.
# 3	Intramedullary canal Fibrous tissue in the union Partially mature bone Chondral ossification of 0.7 mm on both sides (see Figure 5.9)	4.5mm.	Union = 3.4 mm No medullary canal Calcified hematoma Chondral ossification Fibrous tissue = 0.4 mm	3.5mm.
# 4	Pseudoarthrosis Synovial tissue and fluid Fibrocartilaginous metaplasia Bone resorption (see Figure 5.10)	6 mm.	Union, no medullary canal No remodelling Bone marrow element Chondral ossification of 0.2 mm, multifocal	4 mm.
# 5	Pseudoarthrosis Rice bodies in synovial tissue and synovial fluid Fibrocartilaginous metaplasia Bone resorption	7 mm.	Union Medullary canal Remodeling, multifocal Chondral ossification of 0.6 mm	4 mm.
# 6	Pseudoarthrosis Fibrocartilaginous tissue Osteoclastic resorption Chondral ossification	2 mm.	Union Medullary canal Full remodelling on one side	3.5mm.
# 7	Union, osteomyelitis	2 mm.	Union, osteomyelitis Fibrocartilaginous foci	2 mm.

Table 5.13.
Histological examination of Group II

No.	Right Femur		Left Femur	
	Evaluations	Callus Width	Evaluations	Callus Width
# 1	NA	NA	NA	NA
# 2	Unorganized hematoma Fibrous tissue Woven bone Chondral ossification of 1.5 mm. (see Figure 5.7)	5 mm.	Medullary canal = 0.4 mm Fibrous tissue Bone marrow = 1.6 mm (see Figure 5.8)	3 mm.
# 3	Intramedullary canal Fibrous tissue in the union Partially mature bone Chondral ossification of 0.7 mm on both sides (see Figure 5.9)	4.5mm.	Union = 3.4 mm No medullary canal Calcified hematoma Chondral ossification Fibrous tissue = 0.4 mm	3.5mm.
# 4	Pseudoarthrosis Synovial tissue and fluid Fibrocartilaginous metaplasia Bone resorption (see Figure 5.10)	6 mm.	Union, no medullary canal No remodelling Bone marrow element Chondral ossification of 0.2 mm, multifocal	4 mm.
# 5	Pseudoarthrosis Rice bodies in synovial tissue and synovial fluid Fibrocartilaginous metaplasia Bone resorption	7 mm.	Union Medullary canal Remodeling, multifocal Chondral ossification of 0.6 mm	4 mm.
# 6	Pseudoarthrosis Fibrocartilaginous tissue Osteoclastic resorption Chondral ossification	2 mm.	Union Medullary canal Full remodelling on one side	3.5mm.
# 7	Union, osteomyelitis	2 mm.	Union, osteomyelitis Fibrocartilaginous foci	2 mm.

Evaluations on the histology of the femurs of Group II and their callus width are listed in Table 5.13. Animal #1 was not studied histologically. Pseudoarthrosis was observed in the right femurs of animals #4, #5 and #6, along with fibrocartilaginous metaplasia, rice bodies, synovial fluid and osteoclastic resorption. Right femurs of animals #2, #3 and #7 and the untreated left femurs of this group displayed a more advanced stage of bone healing. Femurs of this group scored higher on the histological parameters, and were at a more advanced stage of bone healing than those of Group I. Chondral ossification was observed in the bones with unions. Medullary canal formation and full cortex remodeling were more prominent among the femurs of this group.

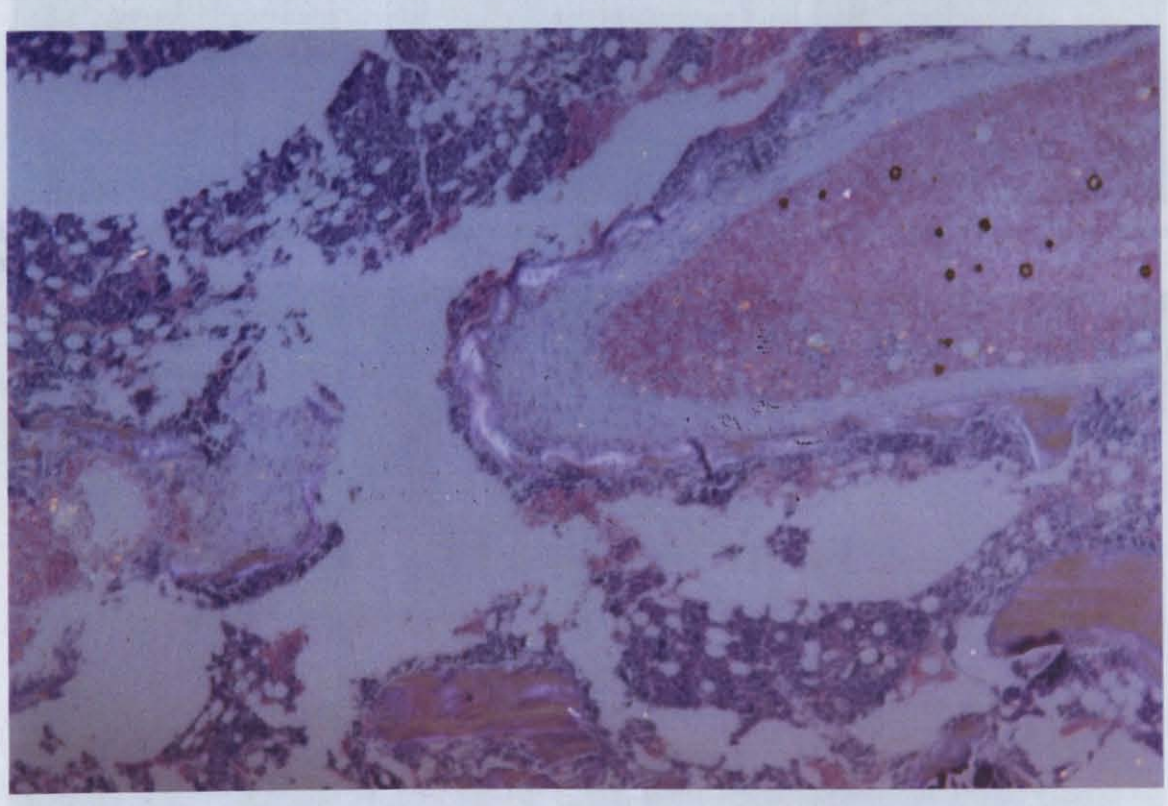

Figure 5.7 Histological section, Group II, animal #2 right femur, H+E stain, 40x, calcified hematoma.

Figure 5.8 Histological section, Group II, animal #2 left femur, H+E stain, 40x, woven bone, chondral ossification.

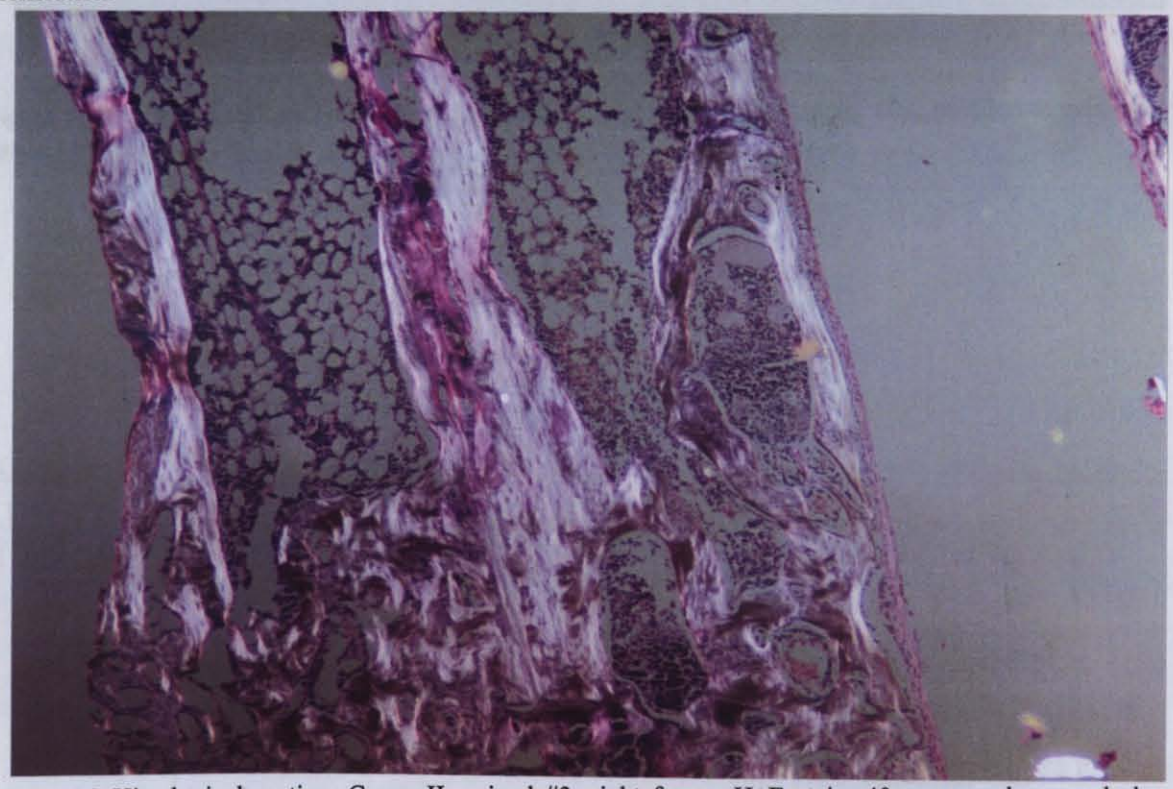

Figure 5.9 Histological section, Group II, animal #3, right femur, H+E stain, 40x, woven bone and chondral ossification.

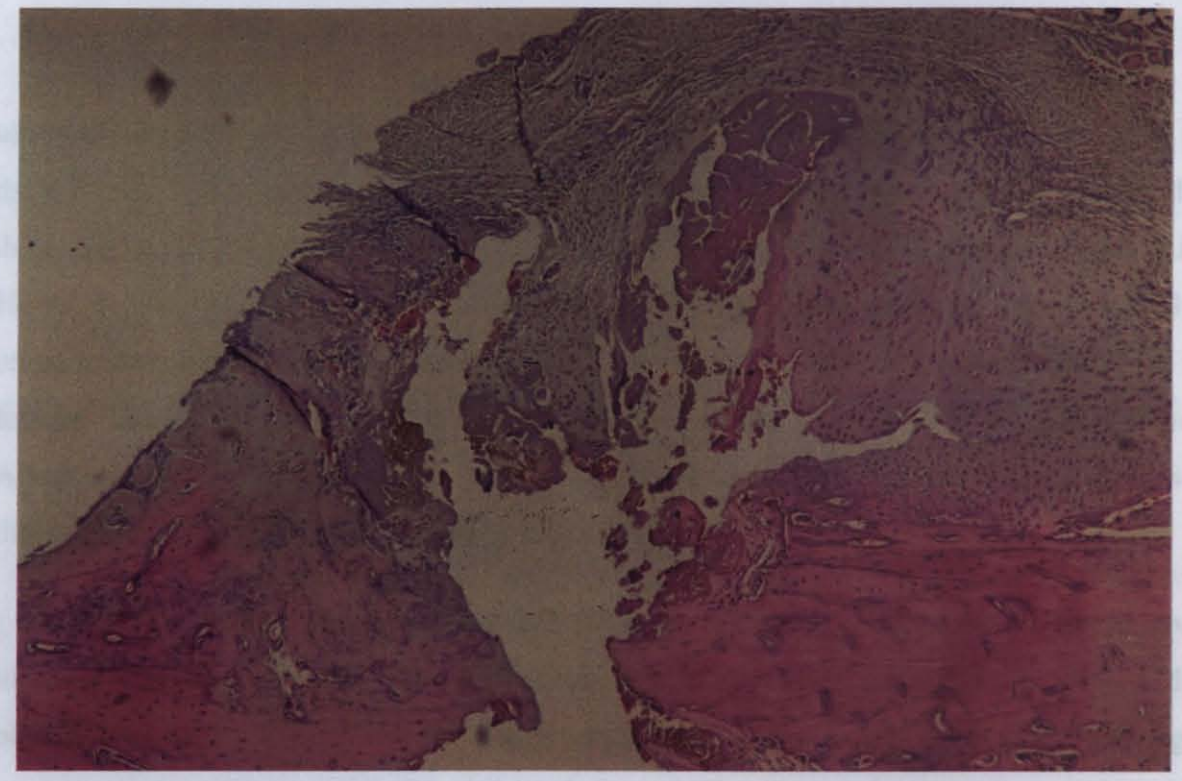

Figure 5.10 Histological section, Group II, animal #4, right femur, H+E stain, 40x, pseudoarthrosis, synovial tissue.

6. DISCUSSION

In assessment of the effectiveness of any method used to enhance bone healing, the ultimate criterion is the presence of a union. At the time of the termination of this study (on the 64th day of the osteotomies), theoretically speaking, the femurs would have been in their third stage of bone healing, by when, an adequately healing bone would have attained a union. However, radiological analysis indicated that among the bones in Group I there was 30% union in both femurs, and 20% union in the right femurs, with 43% of the nonunions in the left femurs. Group II had 85.7% bone union in both femurs and 71.4% union in the right femurs. All of the nonunions in this group were in the right femurs. Macroscopic inspection showed that bone healing in Group II was superior to Group I.

It is expected that an adequately healing bone, in the third healing phase, would have a total radiological score of 8. The radiological scoring of bone healing, done by orthopaedists blind to the study, showed that the average radiological score of Group II (5.81) was again superior to that of Group I (2.87). Student's t-test [47] indicates that there is a difference of 90% significance between the right femurs scores of the groups. The high number of nonunions in the right femurs of Group I lowered the score for this group by not only lowering the radiological score for that leg, but also by retarding the healing of the left femur, thus reducing the overall group radiological score.

In experimental studies, CT and DEXA are used in determining the properties of fracture callus and the state of bone healing. It has been shown that with CT analysis, it is possible to detect the different phases of bone healing, thus making computerized tomographic assessment of fracture callus superior to conventional X-Ray [49]. Experimentally, ESWT is known to increase callus size [29], which reaches a maximum two weeks after fracture and is considered to be an indicator of the degree of healing. However, it is also known that a large callus size may be associated with secondary axial displacement, or incorrect angulation. In addition, callus size has been shown to be unrelated to bone mechanical properties [51], and healing properties [28,29]. In CT analysis, the average callus area of Group I (1.034 mm^2) was

found to be 7.6 times greater than that of Group II (0.136 mm^2), and the total callus area of right femurs in the first group was larger than that of the second group. However, radiological and macroscopic examination of bones indicated superior bone healing in the second group. These results point to the fact that the larger callus size of the first group is due to the higher number of bone nonunions and secondary axial displacements in this group and is not an indicator of the quality of bone healing, supporting the similar findings of McCormack [29], den Boer [51], and Uslu [28].

Callus density and the stiffness of bone increase linearly with calcium content, till about 6 weeks after osteotomy [51]. In callus density measurements, the average density of image pixel is expected to increase with mineralization. Knowing that the bones in the second group are at a more advanced stage of healing and mineralization, a higher mineral density of the callus of the second group was expected. Contrary to our expectation, the average density of image pixel of the second group (-153 to 168) was lower than that of the first group (-170 to 560). The smallness of area of ROI in the second group, and the resulting sampling site variation, reducing the precision of the measured density, may have lowered the value of average density of image pixel. Within the group analysis of callus density indicated expected results: in Group I, a higher density in the femurs with unions when compared to those with nonunions; and in Group II, a relatively higher density in the untreated left femurs when compared to the treated right femurs. Knowing that mineralization of the callus increases over time to provide the rigidity needed for the remodeling phase of bone healing to start, and that with resorption a lower bone density is observed, we think that lower density of image pixel in the second group may also be indicative of the more advanced (remodeling) stage of bone healing.

DEXA analysis of bone is a very practical diagnostic instrument to use in bone density measurements [52]. DEXA analysis gives information about BMC, bone area, and BMD, within the ROI, which must be outlined by one operator in order to prevent person to person variation, because the bone mineral density is calculated by dividing BMC by the area of ROI. The presence of nonunions can further complicate the acquisition of DEXA data: the gap

between the fragmented bone ends, should not be defined within the ROI in order to prevent any errors. Due to the high number of nonunions, in order to attain the best interpretation of results, both BMC and BMD were taken into consideration.

The average BMC of bones of Group II was higher than that of Group I. This may be the result of the higher number of nonunions, lowering the BMC of the bones in the first group, (with the only exception of animal #5, which had the highest BMC and BMD among the bones in both groups). In the second group, the fourth animal, which had a nonunion, had the lowest BMC of this group. The within the group DEXA analysis of bones of the first group shows that both the average BMC, (0.131) and the average BMD (0.076) of treated femurs were lower than the average BMC (0.157) and average BMD (0.089) of untreated femurs. Within the group DEXA analysis of bones in the second group shows that the average BMC (0.114) and average BMD (0.076) of treated femurs were only slightly lower than the average BMC (0.115) and average BMD (0.077) of untreated femurs. The fact that there is no significant difference in both the mineral content and the mineral density of treated and untreated bones may be explained by the fact that bone has to attain a certain BMC and BMD in order to maintain its integrity. With a closer look at the results, the slightly higher BMC and BMD values in some of the right femurs of the second group can also be noticed. However, these slight differences are not statistically significant.

The averages of histological scores for Group II are higher than that of Group I. The histological assessment of the femurs indicate a higher incidence of pseudoarthrosis in Group I, where all of the bones except for the right femur of animal #5, had a developed callus tissue, without any bone union. Synovial tissue, fibrocartilaginous metaplasia, calcified hematoma, granulation tissue, rice bodies, and prominent osteoclastic resorption and in some of the bones suprative osteomyelitis were observed. Similarly, in Group II, femurs with pseudoarthrosis (animals #4, #5, and #6) contained synovial tissue, rice bodies, calcified hematoma, fibrocartilaginous metaplasia and bone resorption. These animals obtained lower histological scores on their right femurs (score of 4 each), than their left femurs (scores of 8, 8 and 10 respectively). The left femurs had a fully developed callus, with bone union. The replacement

of fibrous tissue with new bone marrow, as well as remodeling in some femurs had begun. Both immature and mature bone, and chondral ossification were observed.

In summary, the results of all of the methods used in the assessment of bone healing by ESWT, are in agreement with each other. The results of macroscopic examination are supported by radiological (X-Ray, CT, and DEXA) and histological data: that bone healing in Group II is superior to that of Group I, that despite the group they are from, femurs with pseudoarthrosis have lower scores than femurs with unions, and that the large callus size is not an indicator of the quality of bone healing. The histological findings have made a more finely defined assessment of results possible; by presenting information that had not been displayed by any other assessment method: the pseudoarthrosis in the right femur of animal #6 in Group II. Superior healing of untreated femurs in both groups to treated femurs of Group I and to the pseudoarthritic animals #4, #5 and #6 in Group II is also very clearly indicated by histological studies.

The small sampling size of the experimented group, and the absence of a protocol dictating the total energy to be applied according to bone size and animal species may be listed as the limitations of this study. The presence of three cases with pseudoarthrosis in the second group shows that a treatment using 500 shock waves may still be inadequate for rats of this size and weight. Since the effects of applied energy are related to the physical properties of the experimented animal, i.e. weight, size, femur length, cortical thickness at mid diaphysis, and mineral ash content of the species, the doses applied in previous experiments were taken as references. Variation in the physical properties of the animals presented us a handicap in interpreting the results of the experiment. For example, although the right femur radiological scores of the second group were higher than that of the first group, three animals in the second group had nonunions and displayed a post-traumatic appearance. On the other hand, one animal in the first group displayed close to normal healing of both femurs. In terms of height, size and weight, this animal was the largest of both groups.

7. CONCLUSIONS and FUTURE WORK

Statistically insignificant, yet observable and pronounced quantitative differences between the results of the two groups indicate that ESWT applied at the end of the third week of osteotomies as 1500 shockwaves/treatment at 10 kV had a traumatic effect on rat femur, and that ESW application of 500 shockwaves/treatment at 10 kV neither significantly retarded nor promoted healing of bone tissue. The right femurs of Group II displayed equivalent healing as that of control group consisting of left femurs. However, since traumatic appearance and pseudoarthrosis were observed in three of the treated femurs of Group II, even this energy level may still have a strong dispersing effect on the callus of cortical bones of this size and thickness. Therefore, ESWT must be administered at lower total energy levels in order not to promote pseudoarthrosis. The fact that the untreated bones of the control group displayed growth retardation, it may be stated that ESWT has a more systemic effect than local.

We confirm the findings of McCormack [29], den Boer [51] and Uslu [28], and state that in treatment of osteotomies using ESWT, callus size is not an indicator of bone healing.

In conclusion, the effects of different levels of mechanical energy on the callus were determined; however, the adequate level of energy needed to promote osteogenesis still needs to be studied at lower energy levels.

For future work, the number of treatment sessions used to administer the total energy, and the progress of bone healing over time may be studied at a cellular level, by examining the effect of ESWT on osteogenesis using transgenic mice to dissociate between bone resorption and bone formation as shown by Corral [53].

REFERENCES

1. Haupt, G., A. Haupt, A. Ekkernkamp, B. Gerety, and M. Chvapil, "Influence of Shock Waves on Fracture Healing," *Endourology*, Vol. 39, pp. 529-532, 1992.

2. Brümmer, F., D. Suhr, and D.F. Hülser, "Sensitivity of Normal and Malignant Cells to Shock Waves," *Journal of Stone Disease*, Vol. 4, pp. 243-248, 1992.

3. Brümmer, F., T. Bräuner, and D.F. Hülser, "Biological Effects of Shockwaves," *World Journal of Urology*, Vol. 8, pp. 224-232, 1990.

4. Delius, M., "Medical Applications and Bioeffects of Extracorporeal Shock Waves," *Shock Waves*, Vol. 4, pp. 55-72, 1994.

5. Vogel, J., J. Rompe, C. Hopf, and J. Heine, "High Energy ESW Therapy for Pseudoarthrosis," *1st International Congress of the ESMST*, İzmir-Turkey, 01.06.1998, Memorandum No. P1.646, 1998.

6. Kaulesar-Sukul D.M.K.S., E.J. Johannes, E.G.J.M. Pierik, G.J.W.M. van Eijick, and M.J.E. Kristeljn, "The Effect of High Energy Shock Waves Focused on Cortical Bone: An *in Vitro* Study," *Journal of Surgical Research*, Vol.54, pp. 46-51, 1993.

7. Steinbach, P, F. Hofstädter, H. Nicolai, W. Rössler, and W. Wieland, "*In Vitro* Investigations on Cellular Damage Induced by High Energy Shock Waves," *Ultrasound in Medicine and Biology*, Vol. 18, pp. 691-699, 1992.

8. Haupt, G., "Use of Extracorporeal Shock Waves in the Treatment of Pseudoarthrosis, Tendinopathy and Other Orthopaedic Diseases," *Journal of Urology*, Vol. 158, pp. 4-11, 1997.

9. Beutler, S., G. Regel, H.C. Pape, S. Machtens, A.M. Weinberg, I. Kremeike, U. Jonas, and H. Tscerne, "Die Extrakorporale Stoßwellentherapie (ESWT) in der Behandlung von Pseudoarthrosen des Röhrenknochens, *Unfallchirurg*, Vol. 102, pp. 839-847, 1999.

10. Haupt, G., "Basic Animal Experiments for Orthopaedic Shock Wave Applications," *Journal of Mineral Stoffwechs,* Special Edition, Vol.5, pp. 28-30, 1996.

11. Johannes, E.J., D.M.K.S. Kaulesar-Sukul, and E. Matura, "High-Energy Shock Waves for the Treatment of Nonunions: An Experiment on Dogs," *Journal of Surgical Research*, Vol. 57, pp. 246-252, 1994.

12. Kuderna, H and W. Schaden, "Single Application of Extracorporeal Shockwaves in Delayed Healing Fractures and in Non-Unions," *Journal of Mineral Stoffwechs*, Special Edition, Vol. 5, pp. 35-36, 1996.

13. Russo, S., S. Gigliotti, C. de Durante, R. Canero, and B. Corrado, "Treatment of Nonunion With Shock Waves With Special Reference to Carpal Scaphoid Nonunion," *Applications of shock waves at the bone: Clinical and experimental experiences - Abstract tape of the symposium to the shock wave therapy,* Kassel-Germany, 11-12 April 1997, pp. 40–45, Hamburg, Dr. Kovac Publishing House, 1997.

14. Schaden, W., A. Meznik, F. Russe, and A. Pachucki, "Application of (ESWT) on 40 Patients With Pseudoarthosis or Delayed Bone Fracture Healing," *Applications of shock waves at the bone: Clinical and experimental experiences - Abstract tape of the symposium to the shock wave therapy,* Kassel-Germany, 11-12 April 1997, pp. 40–45, Hamburg, Dr. Kovac Publishing House, 1997.

15. Schleberger, R. and T. Senge, "Non-invasive Treatment of Long-Bone Pseudoarthrosis by Shockwaves (ESWL)," *Archives of Orthropaedic and Trauma Surgery*, Vol. 111, pp. 224-227, 1992.

16. Schleberger, R., "First Clinical Applications of Extracorporeal Shockwaves (ESW) in Orthopaedics," *Journal of Mineral Stoffwechs,* Special Edition, Vol.5, pp. 32-34, 1996.

17. Yel, M and M.I.S. Kapıcıoğlu, "Şok Dalgası (ESWL) Ortopedide Yeni Bir Tedavi Metodu mu?" *Turkish Journal of Arthroplasty and Arthroscopic Surgery*, Vol. 7, pp. 78-80, 1996.

18. Valchanou, V.D. and P. Michailov, "High Energy Shock Waves in the Treatment of Delayed and Nonunion of Fractures," *International Orthopaedics*, Vol. 15, pp. 181-184, 1991.

19. Martin, R.B., D.B. Burr and N.A. Sharkey, *Skeletal Tissue Mechanics,* Heidelberg: Springer-Verlag, 1998.

20. Coleman, A.J. and J.E. Saunders, "A Review of the Physical Properties and Biological Effects of the High Amplitude Acoustic Fields Used in Extracorporeal Lithotripsy," *Ultrasonics*, Vol. 31, pp. 75-89, 1993.

21. Schultheiß, R., "Basic Principles of Shockwaves," *Journal of Mineral Stoffwechs*, Special Edition, Vol. 5, pp. 22-27, 1996.

22. www.pckmed.com

23. Vergunst, J., "*In Vivo* Assessment of Shock-Wave Pressures," *Gastroenterology*, Vol. 99, pp. 1467-1474, 1990.

24. Loew, M., W. Jurgowski, H.C. Mau, and M. Thomsen, "Treatment of Calcifying Tendinitis of Rotator Cuff by Extracorporeal Shock Waves: A Preliminary Report," *Journal of Shoulder and Elbow Surgery*, Vol. 4, pp. 96-106, 1995.

25. Rompe, J.D., F.M. Rumler, C. Hopf, B. Nafe, and J. Heine, "Extracorporeal Shockwave Therapy for Calcifying Tendonitis of the Shoulder," *Clinical Orthopaedics and Related Research*, Vol. 321, pp.196-201, 1995.

26. Yang, C., W.D.W. Heston, S. Gulati, and W.R. Fair, "The Effect of High Energy Shock Waves (HESW) on Human Bone Marrow," *Urological Research*, Vol. 16, pp. 427-429, 1988.

27. Smits, G.A.H.J., P.H.K. Jap, A. Heerschap, G.O.N. Oosterhof, F.M.J. Debruyne, and J.A. Schalken, "Biological Effects of High Energy Shock Waves in Mouse Skeletal Muscle Correlation Between ^{31}P Magnetic Resonance Spectroscopic and Microscopic Alterations," *Ultrasound in Medicine and Biology,* Vol. 19, pp. 399-409, 1993.

28. Uslu, M.M., Ö. Bozdoğan, Ş. Güney, H. Bilgili, Ü. Kaya, B. Olcay, and F. Korkusuz, "The Effect of Extracorporeal Shock Wave Treatment (ESWT) on Bone Defects: An Experimental Study," *Bulletin of Hospital for Joint Diseases*, Vol. 58, pp. 114-118, 1999.

29. McCormack, D., "The Osteogenic Potential of Extracorporeal Shock Wave Therapy. An *in-vivo* study," *Irish Journal of Medical Sciences*, Vol. 165, pp. 20-22, 1996.

30. Gündeş, H., "Yüksek Enerjili Şok Dalgalarının İmmature Kortikal Kemik ve Periost Üzerinde İnvivo Etkileri," M.S. Thesis, Marmara University, 1994.

31. McLean, F.C., and M.R. Urist, *Bone - Fundamentals of the Physiology of Skeletal Tissue,* Chicago: The University of Chicago Press, 1968.

32. Cowin, S.C., W.C. Van Buskirk and R.B. Ashman, "*Properties of Bone*," in R. Skalak and S. Chien (Eds.) *Handbook of Bioengineering*, pp.2.1-2.25, New York: McGraw Hill, 1986.

33. Luciano, D.S., A.J. Wander, J.H. Sherman, *Human Function and Structure*, New York: McGraw Hill, 1978.

34. Coffey, S.A. and L. Klein, "Comparison of Long Bones and Vertebrae in Growing Male Rats: Rate of Growth, Mineralization, and Uptake of ^{3}H-Tetracycline at the Organ Level," *Growth, Development and Aging*, Vol. 52, pp. 151-156, 1988.

35. Rodan, G.A., "Bone Homeostasis," *Proceedings of the National Academy of Sciences, Medical Sciences*, Vol. 95, pp. 13361-13362, 1998.

36. Ravaglioli, A. and A. Krajewski, *Bioceramics, Materials, Properties and Applications*, London: Chapman & Hall, 1992.

37. Johnson, L.C., "Kinetics of Skeletal Remodelling," *Structural Organization of the Skeleton, A Symposium*, Baltimore, Md., USA., November 3, 1965, pp. 66-142.

38. Macdonald, A.G., and P.J. Fraser, "Transduction of Very Small Hydrostatic Pressures," *Comparative Biochemistry and Physiology*, Part A, Vol. 122, pp. 13-36, 1999.

39. Rawlinson, S.C.F., A.A. Pitsillides, and L.E. Lanyon, "Involvement of Different Ion Channels in Osteoblasts' and Osteocytes' Early Responses to Mechanical Strain," *Bone*, Vol. 19, pp. 609-614, 1996.

40. El Haj, A.J., L.M. Walker, M.R. Preston, and S.J. Publicover, "Mechanotransduction Pathways in Bone: Calcium Fluxes and the Role of Voltage-Operated Calcium Channels," *Medical & Biological Engineering & Computing*, Vol. 37, pp. 403-409, 1999.

41. Frost, H.M., and W.S.S. Jee, "A Vital Biomechanical Model of the Endochondral Ossification Mechanism," *The Anatomical Record*, Vol. 240, pp. 435-446, 1994

42. Frost-H.M., and W.S.S. Jee, "Applications of a Biomechanical Model of the Endochondral Ossification Mechanism," *The Anatomical Record*, Vol 240, pp. 447-455, 1994

43. Turner, C.H., "Toward a Mathematical Description of Bone Biology: The Principle of Cellular Accomodation," *Calcified Tissue International*, Vol. 65, pp. 466-471, 1999.

44. Burr, D.B., R.B. Martin, M.B. Schaffler and E.L. Radin, "Bone remodeling in Response to in vivo Fatigue Microdamage," *Journal of Biomechanics*, Vol. 18, pp. 189-200, 1985.

45. Skedros, J. G., S. C. Su, and R.D. Bloebaum, "Biomechanical Implications of Mineral Content and Microstructural Variations in Cortical Bone of Horse, Elk, and Sheep Calcanei," *The Anatomical Record*, Vol. 249, pp. 297-316, 1997.

46. Turner, C.H., "Functional Determinants of Bone Structure: Beyond Wolff's Law of Bone Transformation," *Bone*, Vol. 13, pp. 403-409, 1992.

47. Mould, R.F., *Introductory Medical Statistics,* Bristol: Adam Hilger, 1989.

48. An, Y.H., R.J. Friedman and R.A. Draughn, *Animal Models of Bone Fracture or Osteotomy,"* in An, Y.H. and R.J. Friedman (Eds), *Animal Models in Orthopaedic Research*, pp. 197-217, Boca Raton: CRC Press, 1999.

49. Korkusuz, F., S. Akın, O. Akkuş, and P. Korkusuz, "Assessment of Mineral Density and Atomic Content of Fracture Callus by Quantitative Computerized Tomography," *Journal of Orthopaedic Science*, Vol. 5, pp. 248-255, 2000.

50. www.lunarcorp.com

51. den Boer, E.C., J.A.M. Bramer, P. Patka, F.C. Bakker, R.H. Barentsen, A.J. Feilzer, E.S.M. de Lange, and H.J.T.M. Haarman, "Quantification of Fracture Healing with Three-dimensional Computed Tomography," *Archives of Orthopaedic and Trauma Surgery*, Vol. 117, pp. 345-350, 1998.

52. Jarvinen, T.L.N., H. Sievanen, P. Kannus, and M.Jarvinen, "Dual-Energy X-Ray Absorptiometry in Predicting Mechanical Characteristics of Rat Femur, *Bone*, Vol. 22, pp. 551-558, 1998.

53. Corral, D.A., M. Amling, M. Priemel, E. Loyer, S. Fuchs, P. Ducy, R. Baron, and G. Karsenty, "Dissociation Between Bone Resorption and Bone Formation in Osteopenic Transgenic Mice," *Proceedings of the National Academy of Sciences, Medical Sciences*, Vol. 95, pp. 13835-13840, 1998.